Am J Physiol Cell Physiol 284: C918–C933, 2003.
First published December 27, 2002; 10.1152/ajpcell.00464.2002.

Secretory activation of basolateral membrane Cl^- channels in guinea pig distal colonic crypts

Yingjun Li, Susan Troutman Halm, and Dan R. Halm
Department of Physiology and Biophysics, Wright State University, Dayton, Ohio 45435

Submitted 3 October 2002; accepted in final form 5 December 2002

Li, Yingjun, Susan Troutman Halm, and Dan R. Halm. Secretory activation of basolateral membrane Cl^- channels in guinea pig distal colonic crypts. *Am J Physiol Cell Physiol* 284: C918–C933, 2003. First published December 27, 2002; 10.1152/ajpcell.00464.2002.—Cell-attached recordings revealed Cl^- channel activity in basolateral membrane of guinea pig distal colonic crypts isolated from basement membrane. Outwardly rectified currents ($^{gp}Cl_{or}$) were apparent with a single-channel conductance (γ) of 29 pS at resting membrane electrical potential; another outward rectifier with γ of 24 pS was also observed (~25% of $^{gp}Cl_{or}$). At a holding potential of −80 mV γ was 18 pS for both $^{gp}Cl_{or}$ currents, and at +80 mV γ was 67 and 40 pS, respectively. Identity as Cl^- channels was confirmed in excised patches by changing bath ion composition. From reversal potentials, relative permeability of K^+ over Cl^- (P_K/P_{Cl}) was 0.07 ± 0.03, with relative permeability of Na^+ over Cl^- (P_{Na}/P_{Cl}) = 0.08 ± 0.04. A second type of Cl^- channel was seen with linear current-voltage (*I-V*) relations ($^{gp}Cl_L$), having subtypes with γ of 21, 13, and 8 pS. Epinephrine or forskolin increased the number of open $^{gp}Cl_{or}$ and $^{gp}Cl_L$. Open probabilities (P_o) of $^{gp}Cl_{or}$, $^{gp}Cl_{L21}$, and $^{gp}Cl_{L13}$ were voltage dependent in cell-attached patches, higher at more positive potentials. Kinetics of $^{gp}Cl_{or}$ were more rapid with epinephrine activation than with forskolin activation. Epinephrine increased P_o at the resting membrane potential for $^{gp}Cl_{L13}$. Secretagogue activation of these Cl^- channels may contribute to stimulation of electrogenic K^+ secretion across colonic epithelium by increasing basolateral membrane Cl^- conductance that permits Cl^- exit after uptake via Na^+-K^+-$2Cl^-$ cotransport.

potassium ion secretion; chloride secretion; epinephrine; prostaglandin E_2; forskolin

EPITHELIAL ION SECRETION DRIVES fluid secretion by producing transepithelial osmotic gradients (8, 18, 19). Electrogenic Cl^- secretion is a common type of transport in these fluid secretory epithelia. The cellular mechanism for this secretion includes Cl^- channels in the apical membrane that are activated by various secretagogues through the action of intracellular signaling pathways. Colonic epithelia of mammals also produce electrogenic K^+ secretion via a cellular mechanism similar to that for Cl^- secretion except that apical Cl^- conductance is not activated (17, 19, 23, 50, 51). Secretagogues producing electrogenic K^+ secretion with little or no accompanying steady-state Cl^- secretion include epinephrine (17, 19, 50, 68), prostaglandin E_2 (PGE_2) (23, 50), aldosterone (21, 51), and cholinergic agonists such as carbachol (6, 11). Sensitivity of this K^+ secretion to bumetanide (17, 50, 51, 68) supports a requirement for basolateral membrane Na^+-K^+-$2Cl^-$ cotransporters. Because Cl^- entering together with Na^+ and K^+ does not exit into the lumen, a second basolateral Cl^- transport process is necessary to allow maintenance of intracellular Cl^- concentration during steady-state K^+ secretion (24, 27). Inhibition of K^+ secretion by DIDS further supports that another basolateral Cl^- transport pathway is involved (17). Basolateral membrane Cl^- channels have been proposed as this Cl^- exit step that would contribute to the observed positive charge flow across the epithelium from blood side to lumen (17). Activation of basolateral membrane Cl^- channels as well as apical membrane K^+ channels presumably would occur during secretagogue stimulation to initiate and sustain steady-state electrogenic K^+ secretion.

Basolateral membrane Cl^- conductance (g_b^{Cl}) serves multiple functions in epithelial cells. Electrolyte absorption in the thick ascending limb of Henle's loop (52) and in the intestine of teleost fish (25) uses a cellular mechanism in which Cl^- enters across the apical membrane via Na^+-K^+-$2Cl^-$ cotransporters and exits, in part, through basolateral membrane Cl^- channels. The cochlea and vestibular labyrinth of the inner ear secrete K^+ by a mechanism (67) similar to that proposed for the colonic epithelium (17). In addition, g_b^{Cl} is activated during regulatory volume decrease in colonic crypts as well as other cell types (12, 47, 57, 62). Similarities may exist for the control of Cl^- channels during transepithelial ion flow and cell volume regulation, but whether the same channels serve both types of function in epithelia has not been determined.

Numerous classes of Cl^- channels have been identified that are involved in transepithelial flow and cell volume control as well as contributing to conductances in specific cells to support synaptic signaling and modulation of excitability (15, 33, 47, 60, 62, 69). Some of these Cl^- channel types are pertinent to epithelial function, and three have a defined molecular identity: CFTR (33, 60), the CLC family (33, 69), and the Ca^{2+}-activated Cl^- channel family CLCA (16). Volume-regulated Cl^- channels (Cl_{vol}) and an outwardly rectified

Address for reprint requests and other correspondence: D. R. Halm, Dept. of Physiology and Biophysics, Wright State Univ., 3640 Colonel Glenn Hwy., Dayton OH 45435 (E-mail: dan.halm@wright.edu).

The costs of publication of this article were defrayed in part by the payment of page charges. The article must therefore be hereby marked "*advertisement*" in accordance with 18 U.S.C. Section 1734 solely to indicate this fact.

Cl^- channel (Cl_{or}) are of uncertain molecular identity but are present in intestinal epithelia (3, 5, 12, 47, 57, 62). CFTR is a Cl^- channel with voltage-independent single-channel conductance (γ) of ~9 pS activated by cellular protein kinases (33, 60). Members of the CLC family have voltage-dependent currents variously inwardly rectified and outwardly rectified with γ from ~1 pS to >40 pS (33, 52, 69). CLCA is activated by Ca^{2+} with γ of 15–30 pS (16). Cell swelling activates Cl_{vol}, which has outwardly rectified currents with γ of uncertain size (12, 47, 61, 62). The outwardly rectified γ- and depolarization-enhanced open probability (P_o) of Cl_{or} (20, 26, 43, 61) appears to be distinct from that of Cl_{vol} (47, 61, 62). Blockers have been described for these channel types, but most are relatively nonspecific so that defining channel type by blocker sensitivity is problematic at present (33, 47, 48, 58, 61, 62).

Several of these Cl^- channel types have been localized to colonic epithelia. CFTR mRNA is expressed primarily in the lower two-thirds of colonic crypts (63). A basolateral localization of CFTR would be counter to the commonly accepted function as a secretory Cl^- channel, but its presence at low levels in the basolateral membrane of sweat gland duct cells may support Cl^- absorption from the primary sweat (10, 34). CLCA-1 mRNA is expressed in colon, particularly crypt goblet cells (16). In the CLC family CLC-2, CLC-3, CLC-4, CLC-6, and CLC-7 are broadly distributed (33). CLC-2 appears in the basolateral membrane of surface and crypt epithelium in rat colon and at an intracellular location in human colonic crypts (40); in guinea pig distal colon, CLC-2 was localized only to the basolateral membrane of the surface epithelium (7). An intracellular location also is expected for CLC-3, -4, -5, -6, and -7 (33). A splice variant, CLC-3B, is expressed predominantly in epithelia and alters plasma membrane Cl^- conductance (46). CLC-4 colocalizes with CFTR to the apical membrane of rat ileal crypt cells (44); an intracellular localization near the basolateral membrane was apparent for CLC-5 in rat colon (65). CLC-K has been localized to the basolateral membrane in the thick ascending limb of Henle's loop and collecting duct of kidney as well as cochlea and vestibular labyrinth of inner ear (33, 52, 55, 66). Similarly, basolateral Cl^- channels in colonic crypt cells would serve to permit exit of Cl^- from the cell into the interstitial space and thus support electrogenic K^+ secretion. This study provides results indicating that K^+ secretagogues activated basolateral membrane Cl^- channels in colonic crypt cells. The observed stimulation of several Cl^- channel activities, through an increased number of open channels and an increased channel P_o, would lead to greater g_b^{Cl} consistent with an involvement in Cl^- exit during electrogenic K^+ secretion.

METHODS

Male guinea pigs (400- to 700-g body wt) received standard guinea pig chow and water ad libitum. Guinea pigs were killed by decapitation in accordance with a protocol approved by the Wright State University Institutional Laboratory Animal Care and Use Committee. Distal colon was removed and defined as the ~20-cm-long segment ending roughly 5 cm from the rectum. Colonic segments were cut open along the mesenteric line and flushed with ice-cold Ringer solution to remove fecal pellets. Epithelium was separated from underlying submucosa and muscle layers by using a glass slide to gently scrape along the length of the colonic segment. The plane of dissection occurred at the base of the crypts such that only components of the mucosa immediately adherent to the epithelium remained. These isolated colonic mucosal sheets were used for measurement of transepithelial current and conductance (23) as well as for further isolation of intact crypts, allowing patch-clamp recording of basolateral membrane currents (39).

Four mucosal sheets from each animal were mounted in Ussing chambers with an aperture of 0.64 cm^2. These sheets were supported on the serosal face by Nuclepore filters (Whatman) with a thickness of ~10 μm and a pore diameter of 5 μm. Bathing solutions (10 ml) were circulated by gas lift through water-jacketed reservoirs that were maintained at 38°C. Standard Ringer solution contained (in mM) 145 Na^+, 5 K^+, 2 Ca^{2+}, 1.2 Mg^{2+}, 125 Cl^-, 25 HCO_3^-, 4 $H_{(3-x)}PO_4^{X-}$, and 10 D-glucose. Solutions were continually gassed with 95% O_2 and 5% CO_2, which maintained solution pH at 7.4. Transepithelial electrical potential difference (V_t) was measured by two calomel electrodes connected to the chambers by Ringer-agar bridges. Chambers were connected to automatic voltage clamps (Physiologic Instruments, San Diego, CA) that permitted continuous measurement of short-circuit current (I_{sc}) and compensation for solution resistance. Current was passed across the tissue through two Ag-AgCl electrodes connected by Ringer-agar bridges. I_{sc} is described as positive for current flowing across the epithelium from the mucosal side to the serosal side. Transepithelial conductance (G_t) was measured by recording currents resulting from bipolar square voltage pulses (±5 mV, 3-s duration) imposed across the mucosa at 1-min intervals.

Portions of mucosa were mounted with cyanoacrylate glue onto Lucite holders with apertures 1 cm wide and 4 cm long to permit isolation of intact crypts. Mucosal portions on holders were incubated at 38°C in HEPES-buffered solution, with indomethacin (1 μM) to reduce spontaneous fluid and mucus secretion (22, 23, 50). Standard HEPES-buffered Ringer solution contained (in mM) 142 Na^+, 5 K^+, 2 Ca^{2+}, 1.2 Mg^{2+}, 143 Cl^-, 4 $H_{(3-x)}PO_4^{X-}$, 10 HEPES, and 10 D-glucose. Solutions were continually aerated with room air. Isolation of crypts from the mucosa followed general procedures developed previously (39). Solutions for separating epithelium from underlying connective tissue contained (in mM) 192 Na^+, 5 K^+, 97 Cl^-, 4 $H_{(3-x)}PO_4^{X-}$, 10 HEPES, 10 D-glucose, and either 30 mM citrate or EDTA. Isolation solution containing EDTA also had 0.1% bovine serum albumin. Best results were obtained when the EDTA solution was prepared on the day of the isolation, as noted previously (2). Mucosal portions were consecutively incubated in 30 mM citrate Ringer with indomethacin (1 μM) for 15–30 min and 30 mM EDTA Ringer for 15–20 min at 38°C. Holders then were agitated in HEPES-buffered Ringer with indomethacin (1 μM) and dithiothreitol (1 mM) to release surface and crypt epithelium. Inclusion of dithiothreitol reduced clumping of epithelium within extruded mucus. Isolated crypts were stored on ice or in a refrigerator until use. Patch-clamp recording on these crypts began ~2 h after removal of the colon from the animal and were suitable for patch-clamp experiments up to ~36 h.

Isolated crypts were transferred onto a poly-lysine-coated plastic coverslip in the electrical recording chamber mounted on the stage of an inverted microscope (Diaphot, Nikon).

Bathing solutions were perfused into the chamber by a peristaltic pump (Gilson, Middleton, WI), at room temperature. Pipettes were fabricated from 7052 glass (WPI, Sarasota, FL) with a two-stage puller (Narishige, Tokyo, Japan), coated with Q-dope (GC Electronics, Rockford, IL), and fire-polished. Pipettes filled with either high-Na^+ or high-K^+ solution (Table 1) had resistances of 5–10 MΩ and were connected to the head stage of an EPC-7 patch-clamp amplifier (List-Medical) via a 150 mM KCl-agar salt bridge inside a holder containing a Ag/AgCl electrode (14). The reference electrode was a Ag/AgCl pellet connected to the bath through a 150 mM KCl-agar salt bridge. Currents were recorded on videotape with 3-kHz filtering using a pulse code-modulated VCR (Vetter Instruments, Rebersburg, PA). Seals were made on the central tubular portion of isolated crypts bathed in standard HEPES-buffered Ringer solution. Seals of >1 GΩ were obtained in about one of five attempts. Before excision of patches the bath solution was changed to one containing EGTA (Table 1) to maintain low free Ca^{2+} that would mimic maximal intracellular conditions (~10 μM) but be low enough to avoid activation of nonselective cation channels (5). Lower levels of bath free Ca^{2+} (~100 nM and <10 nM) were produced by adding only 0.1 mM Ca^{2+} or no Ca^{2+}, respectively, to these bath solutions. Solution osmolarity was 292 mosM (290–294 mosM), except for the 300 Cl bath.

Drugs were added in small volumes from concentrated stock solutions. PGE_2, indomethacin, and NS-398 were obtained from Cayman Chemical (Ann Arbor, MI) and epinephrine from Elkins-Sinn (Cherry Hill, NJ). All other chemicals were obtained from Sigma (St. Louis, MO). PGE_2 was prepared in an ethanol stock solution that added 0.1% ethanol at 10 μM of PGE_2; additions of 1% ethanol alone did not alter transepithelial measures of K^+ or Cl^- secretion (23).

Data analysis. Concentration responses of I_{sc} and G_t to forskolin were fit to Henri-Michaelis-Menten binding curves with a nonlinear least-squares procedure. Two independent binding curves were required (23), $I = I_A/[1 + (EC^A_{50}/C)] + I_B/[1 + (EC^B_{50}/C)]$ or $G = G_A/[1 + (EC^A_{50}/C)] + G_B/[1 + (EC^B_{50}/C)]$, such that total I_{sc} or G_t was a combination of these two components (I_A and I_B; G_A and G_B) at each concentration (C). Results are reported as means ± SE. Statistical comparisons were made with a two-tailed Student's *t*-test for paired responses, with significant difference accepted at $P < 0.05$.

Patch-clamp current data were transferred via DigiData-1200 interface to a computer for analysis with pCLAMP6 software (Axon Instruments, Foster City, CA). Currents were filtered at 700 Hz. Junction potentials (1, 45) at pipette tip and bath reference bridge were calculated to correct holding potentials (V_{hold}). Relative ion permeabilities were calculated with the Goldman-Hodgkin-Katz potential equation together with the measured reversal potential and solution ion composition. P_o was calculated from all-points histograms of current amplitude. Area (A) under each current peak was determined by a Gaussian fit. P_o was obtained from the relation: $P_o = (\Sigma i A_i)/\Sigma A_i/N$ with i indicating each peak starting at 0 for baseline and increasing to N, the number of active channels. A *I-V* relation was constructed from the lowest current peaks to ensure that the lowest peak at each V_{hold} indicated the closed state. Records of sufficient length (5–10 min) were obtained for each condition to allow a reliable measure of N from the number of observed peaks (29). In records containing only one channel further kinetic analysis was performed by producing histograms of open and closed durations from an events list. For this analysis, current records were sampled at a rate of 20 μs/point and then filtered at 1 kHz to minimize noise but also maximize bandwidth. Log binning was used to improve fitting and display of exponential curves (32); maximal likelihood estimates were used to obtain time constants from open and closed durations.

RESULTS

Isolated crypts had basolateral membranes that were accessible to sealing with patch pipettes; seals were obtained on the middle section of the crypt cylinder. Identity of cells as either columnar or goblet (22) was not readily discernable. Reversal potentials of ionic currents while cell attached aided identification of the channel types producing those currents (39). For crypt epithelial cells, currents from Cl^- and K^+ channels recorded with high-Na^+ pipette solution were expected to reverse at positive and negative V_{hold}, respectively, as determined by the ion concentration gradients (24, 27) together with a cell membrane electrical potential difference (PD) (V_{cell}) of about −65 mV (42). Thus, at resting V_{cell} (V_{hold} = 0 mV), Cl^- currents would be inward (net outward Cl^- flow) and K^+ currents would be outward. In addition, nonselective cation channel currents would reverse at large positive V_{hold} corresponding to a V_{cell} of 0 mV. Using high-K^+ pipette solution (Table 1) has the advantage of shifting the reversal potential for K^+ channels toward a V_{cell} of 0 mV. Reversal of K^+ channel currents near a V_{hold} of +40 mV (39) indicates that resting V_{cell} was about −40 mV in these isolated crypts. The shift in reversal potential for K^+ channels (to V_{cell} = 0 mV) also provided greater separation from the expected Cl^- channel reversal potential.

Spontaneous single-channel currents consistent with Cl^- channel activity were observed while cell attached (Fig. 1) with both high-Na^+ and high-K^+ pipette solutions. Currents from outwardly rectified

Table 1. *Patch-clamp solutions*

Solution	Na^+	K^+	Mg^{2+}	Ca^{2+}	Cl^-	Gluconate$^-$	EGTA
High Na^+ pipette	153	5	1.2	2.0	162		
High K^+ pipette	18	140	1.2	2.0	162		
Na-glcn bath	157.5		5.0	1.0	50	114	1.0
K-glcn bath	14.5	143	5.0	1.0	50	114	1.0
NaCl bath	154.5		5.0	1.0	161.5		1.0
KCl bath	14.5	140	5.0	1.0	161.5		1.0
300NaCl bath	304.5		5.0	1.0	311		1.0
300KCl bath	5.5	300	5.0	1.0	312		1.0

All solutions contained HEPES (5 mM) and were titrated to pH 7.4 for pipette and pH 7.2 for bath solutions. glcn, Gluconate.

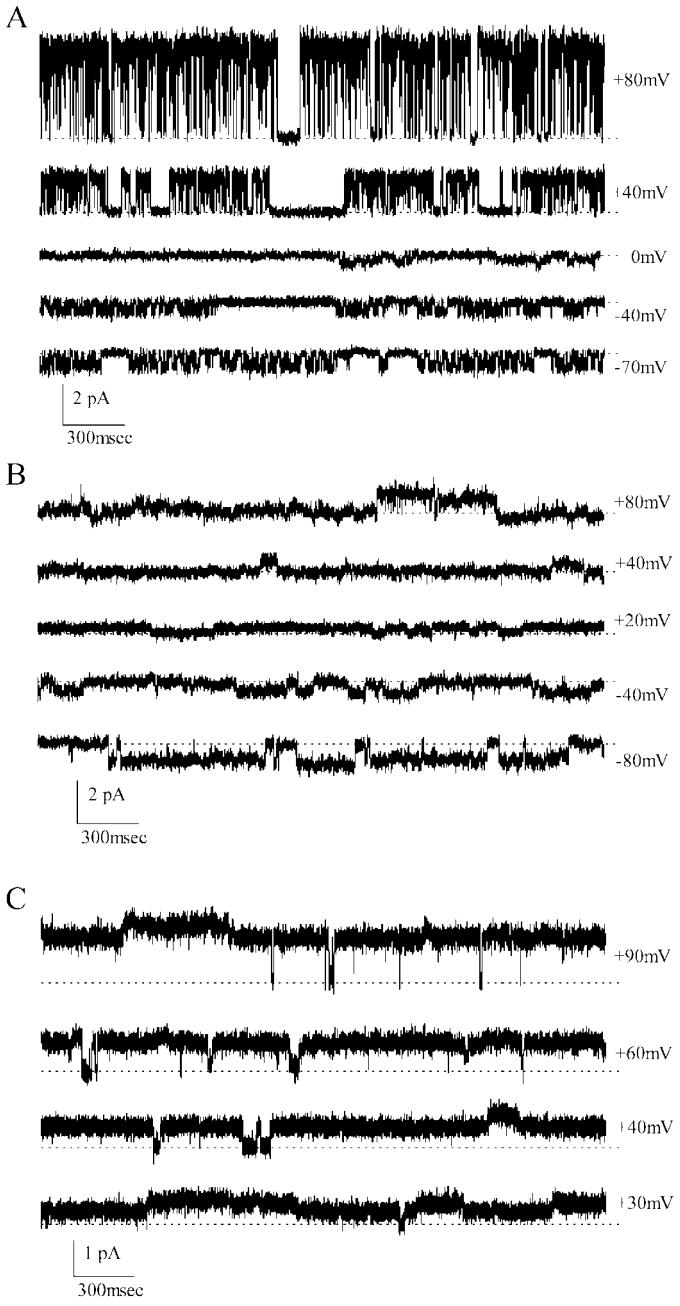

Fig. 1. Cl^- channel currents in crypt cells. Current traces are shown of cell-attached patches from basolateral membrane of isolated colonic crypts. Pipette solution was high-K^+ containing 140 mM K^+ (Table 1). Dashed lines indicate closed state. *A*: an outwardly rectified Cl^- channel ($^{gp}Cl_{or}$) is shown together with an inwardly rectifying K^+ channel ($^{gp}K_{ir}$). Currents from $^{gp}K_{ir}$ reverse near +40 mV, and those for $^{gp}Cl_{or}$ reverse near +5 mV; trace at +80 mV was chosen to show only $^{gp}Cl_{or}$, and traces at negative holding potential (V_{hold}) were chosen to show only $^{gp}K_{ir}$. *B*: current traces are shown for a voltage-independent (linear-γ) Cl^- channel of 12 pS. *C*: current traces are shown for 2 linear-γ Cl^- channels of 6 and 17 pS.

Cl^- channels (Fig. 1*A*) occasionally were seen together with inwardly rectified guinea pig K^+ channels ($^{gp}K_{ir}$; Ref. 39), supporting a resting V_{cell} of about −40 mV in these recordings. Other currents consistent with Cl^- channels also were seen, reversing at V_{hold} of about +5 mV. Several sizes of current events were apparent (Fig. 1, *B* and *C*), generally smaller than the outwardly rectified Cl^- currents. Nonselective cation channels rarely were observed in guinea pig crypts, as noted previously (39).

Outwardly rectified Cl^- channels were seen with two sizes of outward current in guinea pig crypts ($^{gp}Cl_{or}$); inward currents were similar in size (Fig. 2*A*). Activity of $^{gp}Cl_{or}$ was observed in 16 of 231 patches (7%). Cl^- currents (Fig. 2*B*) with linear *I-V* relations ($^{gp}Cl_L$) were observed, congregated into three groups (Fig. 2*C*) on the basis of single-channel γ: 17–25 pS (17 of 231; 7%), 11–15 pS (15 of 231; 6%) and 5–9 pS (10 of 231; 4%). Although these distinctions are somewhat arbitrary, the three groups were clearly separable as indicated by the small variability within each group. The presence of multiple Cl^- channel classes also was supported by appearance of two or more types of $^{gp}Cl_L$ in some patches (Fig. 1*C*), so that differing cell composition alone could not account for the distinct conductances. Cl^- channels were observed in 47 of 231 patches (20%), with more than one Cl^- channel type occasionally present in a single patch (Fig. 1*C*). Positive reversal potentials for $^{gp}Cl_{or}$ and $^{gp}Cl_L$ (Fig. 2, *A* and *B*) support outwardly directed Cl^- flow through these channels at spontaneous V_{cell}, consistent with the predicted requirements for conductive Cl^- flow across the basolateral membrane during electrogenic K^+ secretion.

Cl^- channels were seen together with $^{gp}K_{ir}$ (Fig. 1*A*) and were distinguished by currents exhibiting distinct reversal potentials and rectification. In five patches, $^{gp}Cl_{or}$ was observed together with $^{gp}K_{ir}$. On the basis of the proportion of patches exhibiting each of these channel types (39), four patches would have been expected to contain both $^{gp}Cl_{or}$ and $^{gp}K_{ir}$, assuming uniform channel distribution among patched cells. Preferential localization, of the channel types being compared, to separate cell types would reduce the expected number of joint occurrences. Each of the linear-γ Cl^- channels also was observed with $^{gp}K_{ir}$ (expected number of patches): seven (4) for $^{gp}Cl_{L21}$, seven (4) for $^{gp}Cl_{L13}$, and three (3) for $^{gp}Cl_{L8}$. Appearance of these channels together with $^{gp}K_{ir}$ further supported identification as Cl selective, because nonselective cation currents would have reversed near +40 mV similar to $^{gp}K_{ir}$. The various Cl^- channels, as distinguished by conductance, also were observed together. Presence of linear-γ Cl^- channels together with $^{gp}Cl_{or}$ was observed (expected number of patches): four (1) for $^{gp}Cl_{L21}$, four (1) for $^{gp}Cl_{L13}$, and zero (1) for $^{gp}Cl_{L8}$. The presence together of multiple linear-γ Cl^- channel types also was observed (expected number of patches): three (1) for $^{gp}Cl_{L21}$ with $^{gp}Cl_{L13}$, three (1) for $^{gp}Cl_{L21}$ with $^{gp}Cl_{L8}$, and two (1) for $^{gp}Cl_{L13}$ with $^{gp}Cl_{L8}$. The results suggest a clustering of these basolateral channel types.

Ion selectivity. Activity of $^{gp}Cl_{or}$ often persisted after excision into an inside-out (I/O) configuration (8 of 12 patches; 67%), which permitted ion selectivity to be determined more precisely. Increasing or decreasing bathing solution Cl^- concentration (Table 1) shifted the reversal potential as expected for a Cl^--selective

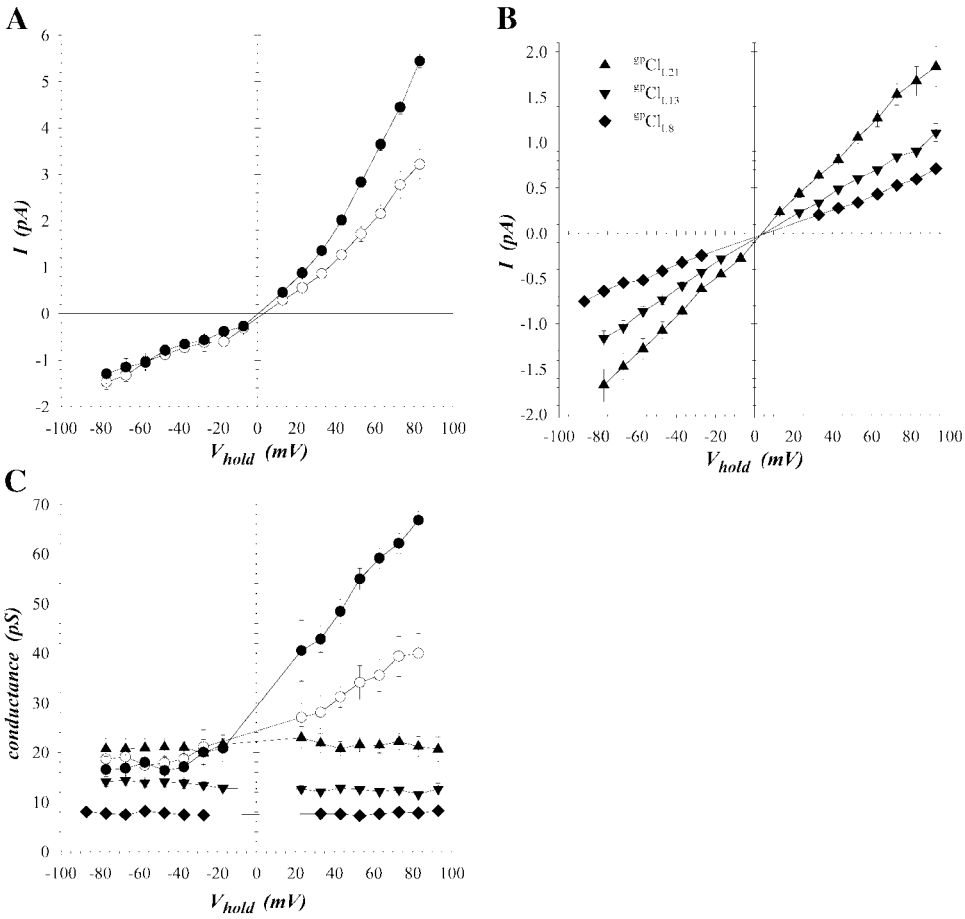

Fig. 2. Cl^- channel conductive properties. *A*: current-voltage (*I-V*) relations are shown (means ± SE) for $^{gp}Cl_{or}$ activity observed in cell-attached patches of crypt basolateral membrane. Two distinct groups were observed, with larger outward currents (●, $n = 9$) and with smaller outward currents (○, $n = 3$). *B*: *I-V* relations are shown for linear-γ Cl^- channel ($^{gp}Cl_L$) activity, exhibiting both inward and outward currents, observed in cell-attached patches of crypt basolateral membrane. Three distinct sizes of activity were observed (◆, $n = 7$; ▼, $n = 10$; ▲, $n = 9$). *C*: single-channel conductance (chord conductance; γ) is shown, from *I-V* relations in *A* and *B*. Mean γ for $^{gp}Cl_{L21}$, $^{gp}Cl_{L13}$, and $^{gp}Cl_{L8}$ was 21.4 ± 1.0, 13.2 ± 0.4, and 8.3 ± 0.5 pS, respectively; each group was significantly different from the other 2 ($P < 0.05$).

channel (Fig. 3*A*). Relative ion permeability was calculated for Cl^- with respect to K^+ and Na^+: relative permeability of K^+ over Cl^- (P_K/P_{Cl}) = 0.07 ± 0.03 ($n = 7$) and relative permeability of Na^+ over Cl^- (P_{Na}/P_{Cl}) = 0.08 ± 0.04 ($n = 4$). Ion selectivity of $^{gp}Cl_L$ was more difficult to determine precisely because these channels generally inactivated on excision; but ion substitution in a few cases ($n = 3$) supported preference for Cl^- over K^+ (data not shown). In addition, excision into symmetrical Cl^- concentrations could be expected to produce inward rectification for $^{gp}Cl_L$; however, activity did not persist in enough cases to resolve the excised *I-V* relations completely.

Increasing Cl^- concentration at the cytoplasmic face of the patch increased γ for $^{gp}Cl_{or}$ at negative V_m (Fig. 3*B*), as expected for conductive Cl^- exit. The dependence of γ on intracellular Cl^- activity ($V_m = -80$ mV) conformed to a Henri-Michaelis-Menten binding curve with γ^{max} of 59 pS and $K_{1/2}$ of 87 mM. This apparent Cl^- affinity for conduction was approximately three-

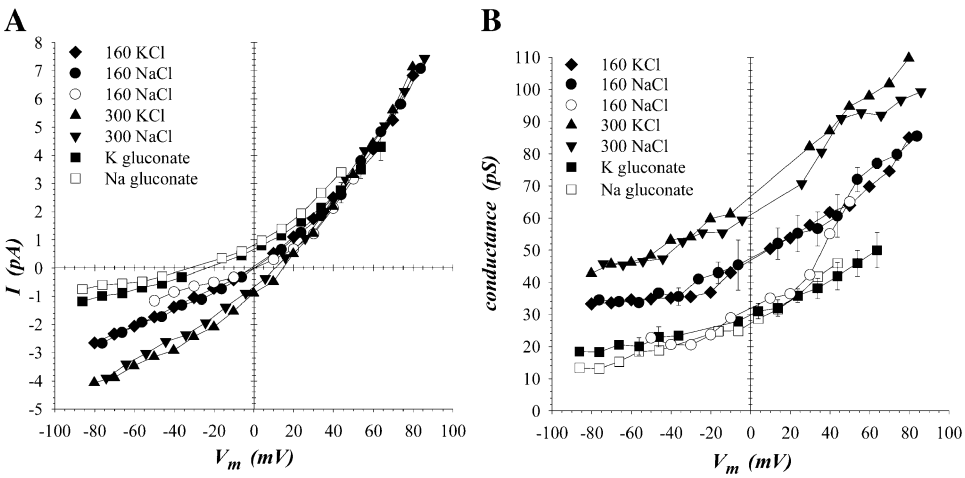

Fig. 3. Ion selectivity of $^{gp}Cl_{or}$. *A*: after excision into inside-out (I/O) configuration, bath solution (Table 1) was changed among NaCl (●, ○; $n = 7, 2$), KCl (◆; $n = 7$), K-gluconate (■; $n = 5$), Na-gluconate (□; $n = 2$), 300 KCl (▲; $n = 2$), and 300 NaCl (▼; $n = 2$). Pipette solution was high-K^+ (filled symbols) or high-Na^+ (open symbols). Bath solutions containing gluconate would have lower Ca^{2+} activities than those with EGTA alone, because of Ca^{2+} binding by gluconate, but $^{gp}Cl_{or}$ activity was not noticeably altered by reduction in Ca^{2+} activity (data not shown). *B*: single-channel conductance (chord conductance) is shown from *I-V* relations in *A*.

fold higher than for $^{T84}Cl_{or}$ (20). The presence of Na^+ in the pipette rather than K^+ (Fig. 3*B*) yielded lower γ at negative V_m when the intracellular Cl^- concentration was 160 mM, but not at 50 mM Cl^-. Comparison of cell-attached currents with those after excision into a low Cl^- concentration that mimics intracellular values (Fig. 4*A*) suggests that the small-γ form of $^{gp}Cl_{or}$ predominated in the excised condition, even though the larger form was more common when cell attached (75%). For the large-γ form of $^{gp}Cl_{or}$, cell-attached γ at negative V_m was similar to the excised γ in 50 mM Cl^- but at positive V_m cell-attached γ was similar to excised γ in 160 mM Cl^- (Fig. 4*B*), further suggesting that γ may be controlled by cytosolic components.

Secretagogue activation of Cl^- channels. Distinct groups of secretagogues stimulate various amounts of electrogenic K^+ and Cl^- secretion across distal colonic epithelia (19, 23). Epinephrine or PGE_2 stimulates electrogenic K^+ secretion, and at higher concentrations PGE_2 also stimulates Cl^- secretion (23, 50). In addition, cholinergic agonists such as carbachol (CCh) stimulate K^+ secretion when added alone but also stimulate Cl^- secretion when added together with other secretagogues such as PGE_2 (6, 11). Forskolin, which increases intracellular cAMP through activation of adenylyl cyclase (4, 64), stimulated a negative I_{sc} across guinea pig distal colonic mucosa (Fig. 5, *A* and *B*), consistent with cation secretion. Identification of this forskolin-stimulated I_{sc} as electrogenic K^+ secretion was supported (Fig. 5) by sensitivity to bumetanide as well as a transepithelial equivalent electromotive force similar to that with other K^+ secretagogues, such as aldosterone, epinephrine, and PGE_2 (21, 23, 50). Also, Ba^{2+} (10 mM) added to the mucosal solution or DIDS (100 μM) added to the serosal solution inhibited forskolin-stimulated I_{sc} and G_t (data not shown), similar to the action on epinephrine-stimulated electrogenic K^+ secretion (17). Forskolin stimulated (Fig. 5, *C* and *D*) negative I_{sc} consistent with K^+ secretion at low concentrations and additionally at higher concentrations positive I_{sc} consistent with Cl^- secretion (50), which mimicked the response to PGE_2 (23, 50) and cAMP (17).

Stimulation of Cl channel activity was measured as increases in number (*N*) and P_o. The conductance (*g*) contributed by each channel type can be calculated from these values together with single-channel conductance, $g = NP_o\gamma$. Spontaneous activity of $^{gp}Cl_{or}$ occurred in 10 of 16 patches with detectable $^{gp}Cl_{or}$ (62%). Linear-γ Cl^- channels occurred spontaneously in 25 of 36 patches with discernable $^{gp}Cl_L$ (69%). These incidence rates overestimate spontaneous activity by ignoring channels that remained resistant to activation because of experimental conditions. This relatively high level of apparently spontaneous Cl^- channel activity in the basolateral membrane is consistent with stimulation of K^+ secretion by low concentrations of PGE_2 and other possible endogenously produced lipid mediators (23).

Epinephrine (5 μM) activated $^{gp}Cl_{or}$ (increased *N*) in 4 of 57 quiescent cell-attached patches (7%), and all were the larger-γ form. Onset was abrupt, with rapid opening and closing kinetics (Fig. 6). PGE_2 (100 nM) failed to activate $^{gp}Cl_{or}$ in 18 quiescent patches (a rate similar to epinephrine would have predicted 1 activated $^{gp}Cl_{or}$). Addition of forskolin (1 μM) to the bath during cell-attached recording (Fig. 7*A*) led to $^{gp}Cl_{or}$ activation (3 of 58 quiescent patches; 5%). Subsequent addition (Fig. 7*B*) of epinephrine (5 μM) activated another $^{gp}Cl_{or}$, PGE_2 (10 μM) addition led to a single $^{gp}Cl_{or}$, and CCh (10 μM) produced erratic current amplitudes together with rapid kinetics. Currents at the beginning of bursts were near the pre-CCh size but declined during the burst. These CCh-attenuated currents at positive V_{hold} had a γ of roughly 60% of the preceding conditions (data not shown). In two other cell-attached patches with active $^{gp}Cl_{or}$, CCh (10 μM) addition in combination with PGE_2 (10 μM) also converted channel kinetics from flickering closures to short openings and closings, but γ was not decreased (data not shown). Reversal potentials for $^{gp}Cl_{or}$ or $^{gp}Cl_L$ were not significantly different among spontaneous and secretagogue-induced conditions (data not shown), indicating an unaltered net driving force for Cl^-. In the combined presence of epinephrine and forskolin (3 patches), the rapid kinetic mode was replaced by the

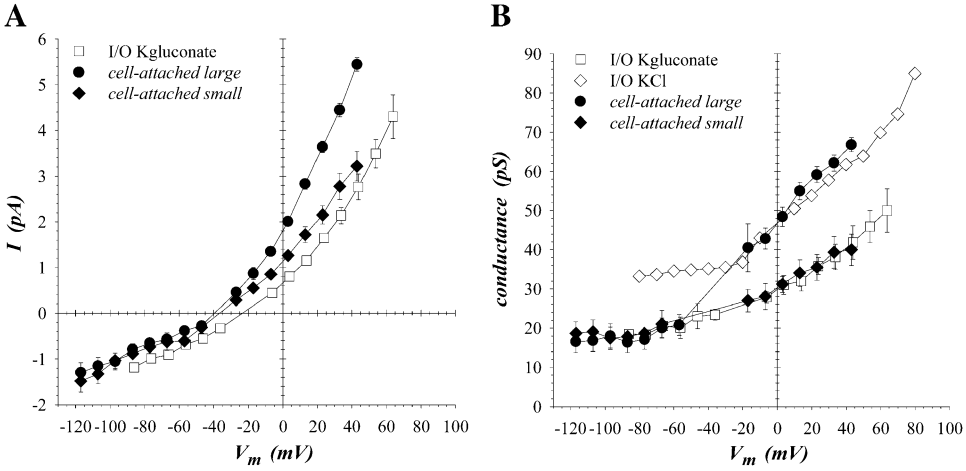

Fig. 4. Conductive properties of $^{gp}Cl_{or}$ after excision. *A*: *I-V* relations are shown for I/O condition with K-gluconate bath (□) together with those for cell-attached condition (Fig. 2*A*) after correction (●, large $^{gp}Cl_{or}$; ◆, small $^{gp}Cl_{or}$) for apparent cell membrane potential difference (V_{cell}) of −40 mV (39), $V_m = V_{hold} + V_{cell}$. Apparent intracellular Cl^- concentration for cell-attached condition was 36 mM, obtained with reversal potentials of corrected currents. *B*: single-channel conductance (chord conductance) is shown from *I-V* relations in *A* together with conductance from Fig. 3*B* (◇, symmetrical KCl).

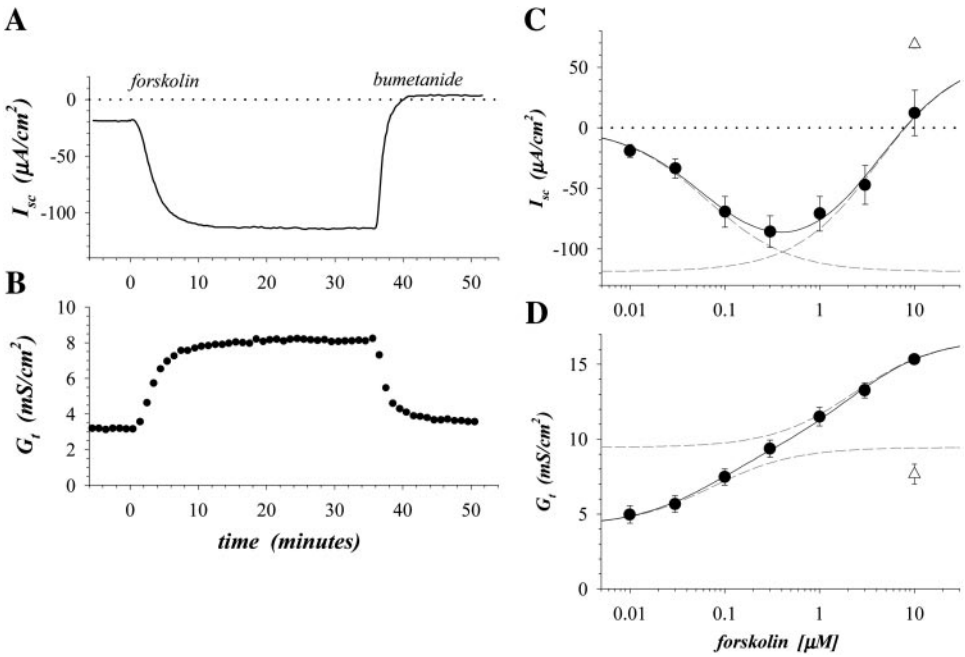

Fig. 5. Forskolin stimulation of K^+ secretion. Short-circuit current (I_{sc}) and transepithelial conductance (G_t) were recorded from guinea pig distal colonic mucosa. Spontaneous rates of ion secretion due to apparent autocrine stimulation (23) were suppressed by repeated (3×) replacement of bathing solutions and addition of cyclooxygenase inhibitors indomethacin (2 μM) and NS-398 (2 μM). Amiloride (100 μM) added to mucosal solution inhibited electrogenic Na^+ absorption. Forskolin (0.3 μM) addition to mucosal and serosal solutions (0 min) stimulated both I_{sc} (*A*) and G_t (*B*). The equivalent electromotive force (EMF = $\Delta I_{sc}/\Delta G_t$) was −24 mV, similar to other K^+ secretagogues (21, 23, 50). Subsequent (35.8 min) serosal addition of bumetanide (100 μM) inhibited both I_{sc} and G_t. Cumulative forskolin concentration responses (n = 7) for I_{sc} (*C*) and G_t (*D*) exhibited 2 saturable components. Solid lines indicate fits for a 2-component model (see METHODS), with high-affinity EC_{50} values of 64 (I_{sc}) and 74 (G_t) nM and low-affinity EC_{50} values of 4.0 (I_{sc}) and 2.3 (G_t) μM. Dashed lines indicate individual fit components; EMF (I_{max}/G_{max}) for high-affinity response was −23 mV and for lower-affinity response was +24 mV. Forskolin-stimulated values after bumetanide (100 μM) addition are also shown (△).

flickering closures characteristic of spontaneous activity (Fig. 7*B*).

Linear-γ Cl^- channels also were activated by K^+ secretagogues. Epinephrine (5 μM) activated (in 57 quiescent patches) $^{gp}Cl_{L21}$ (2; 4%), $^{gp}Cl_{L13}$ (1; 2%), and $^{gp}Cl_{L8}$ (1; 2%). PGE_2 (100 nM) activated (in 18 quiescent patches) $^{gp}Cl_{L21}$ (1; 6%) and $^{gp}Cl_{L13}$ (1; 6%), but not $^{gp}Cl_{L8}$. Forskolin (1 μM) activated (in 58 quiescent patches) $^{gp}Cl_{L21}$ (1; 2%), $^{gp}Cl_{L13}$ (2; 3%), and $^{gp}Cl_{L8}$ (2; 3%). CCh did not have a discernable action on any $^{gp}Cl_L$. Addition of epinephrine or PGE_2 to patches with active $^{gp}Cl_{L13}$ increased channel P_o by reducing the apparent number of long closures (Fig. 8).

The total incidence of Cl^- channel activation (all channel types) by epinephrine (5 μM) was 8 of 57 quiescent cell-attached patches (14%). For PGE_2 (100 nM), the total incidence of Cl^- channel activation was 2 of 18 quiescent patches (11%). The total incidence of Cl^- channel activation with forskolin (1 μM) was 8 of 58 quiescent cell-attached patches (14%). These incidence rates likely underestimate secretagogue sensitivity because many nonresponsive patches may not have contained Cl^- channels. These activation results do support that secretagogues significantly increased g_b^{Cl} but indicate that no particular Cl^- channel type was solely responsible.

P_o of these Cl^- channels was secretagogue dependent. For spontaneously active $^{gp}Cl_{or}$, P_o was lower at negative than at positive V_{hold} (Fig. 9*A*). In the physiological range of V_{cell} (near V_{hold} = 0 mV), P_o was ~0.4. P_o in the forskolin-stimulated state was not detectably different from spontaneous activity, but only values at positive V_{hold} were measurable. Epinephrine activation produced a lower P_o than in the basal or forskolin conditions (Fig. 9*A*), consistent with the briefer open times (Figs. 1*A* and 6*B*); at physiological V_{cell}, P_o of $^{gp}Cl_{or}$ in the epinephrine condition was ~0.2. Spontaneously active $^{gp}Cl_{L21}$ and $^{gp}Cl_{L13}$ also had voltage-dependent P_o, lower at negative V_{hold} with the steepest slope near the spontaneous V_{cell} (Fig. 9*B*). Neither 1 μM forskolin (n = 2) nor 100 nM PGE_2 (n = 1) altered P_o for $^{gp}Cl_{L21}$ (data not shown), but only values at positive V_{hold} were measurable. Stimulation with epinephrine (Fig. 8) or PGE_2 (100 nM) removed the voltage dependence for $^{gp}Cl_{L13}$, such that P_o was ~0.5 (Fig. 9*B*). Spontaneously active $^{gp}Cl_{L8}$ had voltage-independent P_o with a value of either 0.54 ± 0.07 (n = 3) or 0.19 ± 0.04 (n = 3), suggesting the existence of two kinetic modes.

Excision into I/O configuration altered kinetic behavior for $^{gp}Cl_{or}$, perhaps as cytosolic components were lost into the bath solution. Rapid closing kinetics due to

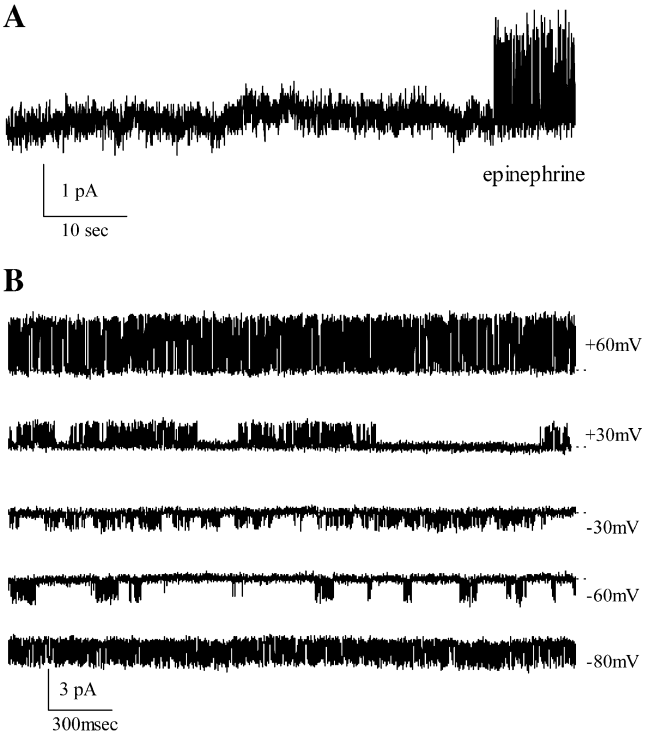

Fig. 6. Epinephrine activation of $^{gp}Cl_{or}$. Currents from $^{gp}Cl_{or}$ were recorded while cell attached. Pipette solution was high-K^+. Dashed lines indicate closed state. *A*: epinephrine (5 μM) was added to the bath solution just before the start of the current trace. Within 1 min $^{gp}Cl_{or}$ became active, after having been quiescent during 17 min of recording in basal condition. V_{hold} was +30 mV. *B*: current traces are shown for $^{gp}Cl_{or}$ activated by epinephrine (*A*).

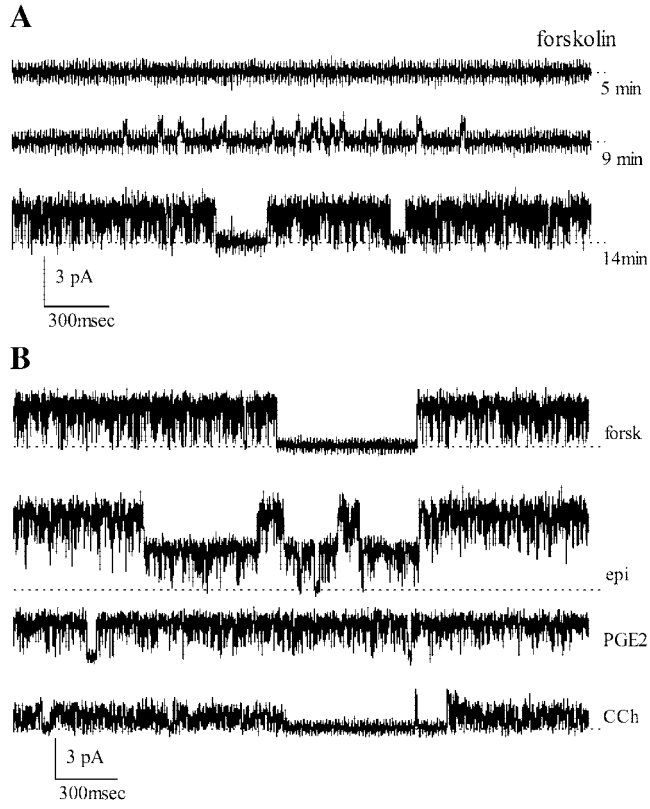

Fig. 7. Forskolin activation of $^{gp}Cl_{or}$. Currents from $^{gp}Cl_{or}$ were recorded while cell attached. Pipette solution was high-K^+. Dashed lines indicate closed state. *A*: $^{gp}Cl_{or}$ became active ~9 min after forskolin (1 μM) addition; V_{hold} was +40 mV. *B*: subsequent addition of epinephrine (5 μM) together with forskolin activated a second $^{gp}Cl_{or}$; cumulative PGE_2 addition (10 μM) led to a single $^{gp}Cl_{or}$; cumulative carbachol (CCh; 10 μM) addition reduced single-channel current amplitude. V_{hold} was +60 mV.

epinephrine activation were slowed such that the channels spent more time open (Fig. 10*A*). In addition, P_o became generally voltage independent after excision with a value of ~0.8 (Fig. 10*B*). Reducing bath solution free Ca^{2+} did not alter P_o of excised $^{gp}Cl_{or}$ (data not shown), similar to previous reports for Cl_{or} (5, 37, 43). Excision of quiescent patches rarely (2 of 231 patches; 1%) led to activation of $^{gp}Cl_{or}$. Activity of all $^{gp}Cl_L$ types generally was lost after excision.

Voltage dependence of γ (Fig. 2*C*) and P_o (Fig. 9*A*) for $^{gp}Cl_{or}$ was used to calculate a time-averaged current that would predict the voltage dependence for a steady-state whole cell current due to $^{gp}Cl_{or}$ (Fig. 11*A*). The combination of voltage dependence from γ and P_o results in a sharp outward rectification; simply multiplying by the number of active channels would reproduce exact whole cell current amplitudes. Voltage dependence of P_o for $^{gp}Cl_{L21}$ and $^{gp}Cl_{L13}$ (Fig. 9*B*) also resulted in time-averaged currents with outward rectification (Fig. 11*B*). Although time-averaged currents from $^{gp}Cl_{or}$ and $^{gp}Cl_{L13}$ are difficult to distinguish, activation of K^+ secretion with epinephrine or low-concentration PGE_2 would evoke a nearly linear time-averaged current from $^{gp}Cl_{L13}$.

Kinetic analysis of $^{gp}Cl_{or}$. Patches with only one $^{gp}Cl_{or}$ present allowed detailed analysis of kinetic behaviors induced by secretagogue activation. Open duration distributions (Fig. 12, *A* and *B*) exhibited two exponentials during spontaneous and forskolin activity, supporting the presence of two open states, but during epinephrine activation distributions had only a single exponential with a shorter time constant (Table 2). Closed duration distributions had three distinct exponentials (Fig. 12, *C* and *D*, and Table 2), consistent with three closed states, and a few long-duration closures (>1 s), suggesting an additional longer-lived closed state of rare occurrence. Closed duration distri-

Fig. 8. Epinephrine stimulation of $^{gp}Cl_{L13}$. Currents from $^{gp}Cl_{L13}$ were recorded while cell attached for the 13 min preceding epinephrine (5 μM) addition. The epinephrine-stimulated trace was recorded 6 min after addition, and similar activity was recorded for an additional 8 min during epinephrine stimulation. Pipette solution was high-K^+. V_{hold} was −60 mV. Dashed lines indicate closed state.

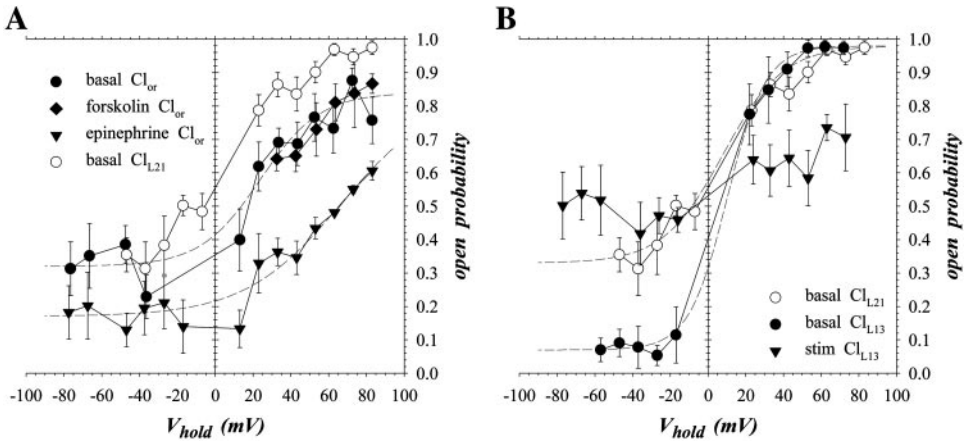

Fig. 9. Cell-attached open probability (P_o). Currents from Cl^- channels were recorded while cell attached before and after secretagogue addition. P_o was calculated from amplitude histograms of current records (see METHODS). Pipette solution was high-K^+. *A*: dependence of $^{gp}Cl_{or}$ P_o on V_{hold} is shown for basal condition (●; $n = 6$) and in the presence of 1 μM forskolin (◆; $n = 3$) or 5 μM epinephrine (▼; $n = 4$). P_o of $^{gp}Cl_{L21}$ for basal condition (○; $n = 3$) is also shown. Fits to Boltzmann distribution (dashed lines) allowed estimates (28) of equivalent gating charge (z_g) and holding voltage at half-activation ($V_{1/2}$) for $^{gp}Cl_{or}$[basal] ($z_g = 1.6$, $V_{1/2} = +22$ mV) and $^{gp}Cl_{or}$[epi] ($z_g = 1.0$, $V_{1/2} = +63$ mV). *B*: dependence of P_o on V_{hold} for spontaneously active $^{gp}Cl_{L21}$ (○; $n = 3$) and $^{gp}Cl_{L13}$ (●; $n = 3$) is shown. Stimulation of $^{gp}Cl_{L13}$ with either epinephrine (5 μM) or low-concentration PGE_2 (100 nM) altered P_o (▼; $n = 3$). Fits to Boltzmann distribution (dashed lines) gave estimates of z_g and $V_{1/2}$ for $^{gp}Cl_{L21}$ ($z_g = 1.6$, $V_{1/2} = +6$ mV) and $^{gp}Cl_{L13}$[basal] ($z_g = 2.5$, $V_{1/2} = +9$ mV).

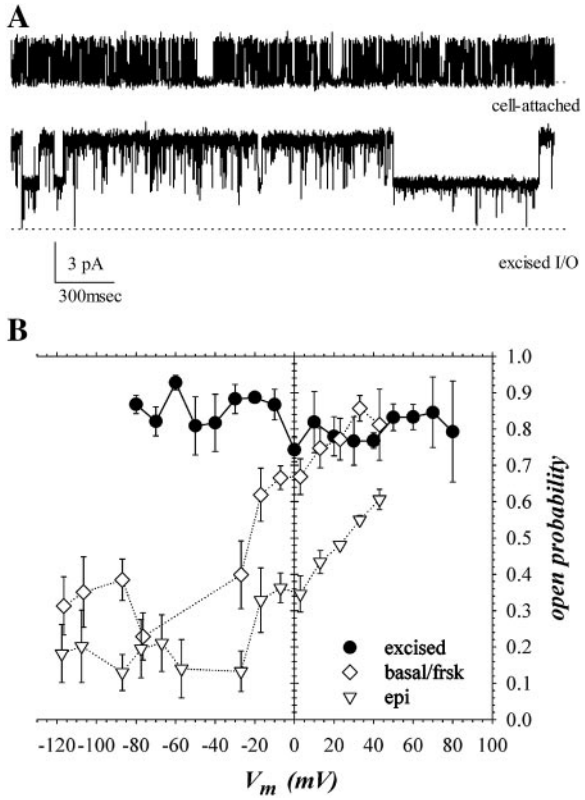

Fig. 10. Excision of $^{gp}Cl_{or}$. *A*: a cell-attached patch with an epinephrine-activated $^{gp}Cl_{or}$ was excised into NaCl bath solution. V_{hold} was +50 mV. Pipette solution was high-K^+. Dashed lines indicate closed state. Openings of 2 $^{gp}Cl_{or}$ were apparent after excision. *B*: P_o of $^{gp}Cl_{or}$ is shown for excised condition (●; $n = 10$). Cell-attached conditions, basal/forskolin (○) and epinephrine (▽) from Fig. 9*A*, are also shown in relation to V_m after correction for apparent V_{cell} of −40 mV (39).

butions differed during epinephrine activation by a shift in events from the short-duration C_1 closed state to the longer-duration C_2 state (Fig. 13 and Table 2). Both the shorter-duration open time and longer-duration closed time during epinephrine activation would contribute to lower P_o (Fig. 9*A*). Thus the powerful K^+ secretagogue epinephrine induced a kinetic mode for $^{gp}Cl_{or}$ distinct from the basal/forskolin kinetic mode.

The time constant (τ) of the most common open events was voltage dependent during spontaneous activity, forskolin activation, and epinephrine activation (Fig. 14). Closed τ were voltage independent, except during epinephrine activation, when one closed time constant (C_2) was voltage dependent (Fig. 14). This extra voltage dependence contributed to the epinephrine-induced shift in the dependence of P_o on voltage (Fig. 9*A*), such that the voltage at half-activation ($V_{1/2}$) was ~40 mV more positive than in the basal/forskolin kinetic mode. The proportion of events making up each open and closed duration exponential was voltage independent (data not shown), within the variations of the measurement (~10%). After excision, the dominant open τ (for long-duration open state) became twofold longer and voltage independent (Table 2 and Fig. 14). Closed τ were similar to basal spontaneous activity (Table 2 and Fig. 13) after excision, supporting the presence of a diffusible mediator controlling the epinephrine-induced closed state distribution.

DISCUSSION

Electrogenic secretion of K^+ across colonic epithelia can occur without accompanying Cl^- secretion or Na^+ absorption and produces a lumen-positive transepithelial electrical potential difference (V_t) via a cellular mechanism (Fig. 15), apparently employing apical

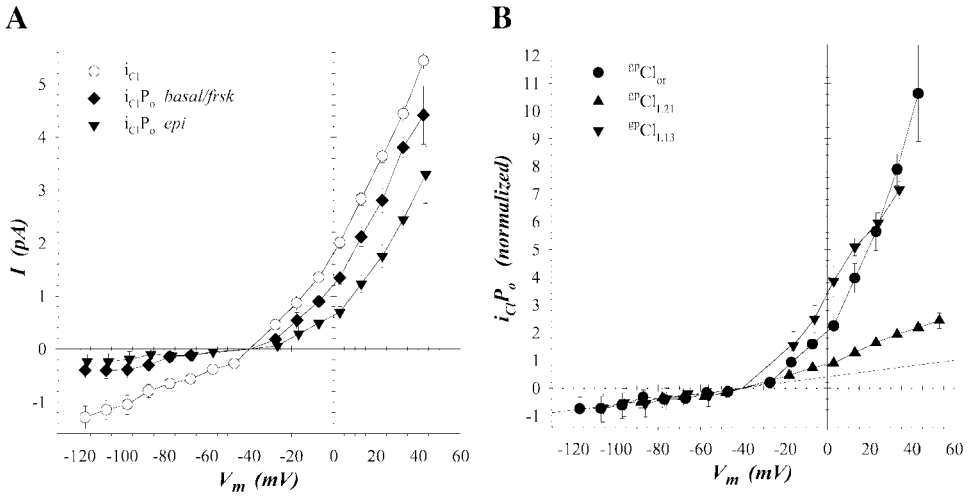

Fig. 11. Time-averaged conductive properties of basolateral membrane Cl^- channels. *A*: *I-V* relation is shown (means ± SE) for $^{gp}Cl_{or}$ activity in cell-attached condition (○; from Fig. 2*A*). Also shown are time-averaged currents, $i_{Cl}P_o$, for basal/forskolin state (◆) and for epinephrine state (▼). Cell-attached P_o from Fig. 9*A* was used to calculate $i_{Cl}P_o$. V_m was calculated from V_{hold} and apparent V_{cell}, −40 mV (39). *B*: time-averaged currents ($i_{Cl}P_o$, calculated from Figs. 2 and 9) are shown for $^{gp}Cl_{or}$[epi] (●), $^{gp}Cl_{L21}$[basal] (▲), $^{gp}Cl_{L13}$[basal] (▼) producing outwardly rectified currents. Currents were normalized to an inward conductance of 10; the dashed line indicates the case for voltage-independent conductance.

membrane K^+ channels and basolateral membrane Cl^- channels (17, 19, 21, 50). Together these conductive pathways contribute to a cell-negative electrical PD at apical (V_a) and basolateral (V_b) membranes that aids in driving basolateral Cl^- exit. Secretory exit of K^+ into the lumen is dependent on the relative K^+ conductance of apical and basolateral membranes as well as the electrochemical driving forces (39, 42, 50). Basolateral exit of Cl^- is essential during this type of K^+ secretion because basolateral Na^+/K^+ pumps drive K^+ uptake via continual extrusion of Na^+ entering through basolateral Na^+-K^+-$2Cl^-$ cotransporters, which results in Cl^- entry (19). Maintenance of cell volume during sustained secretion requires a balance between these basolateral influx and efflux pathways for Cl^- (Fig. 15). Activation by K^+ secretagogues indi-

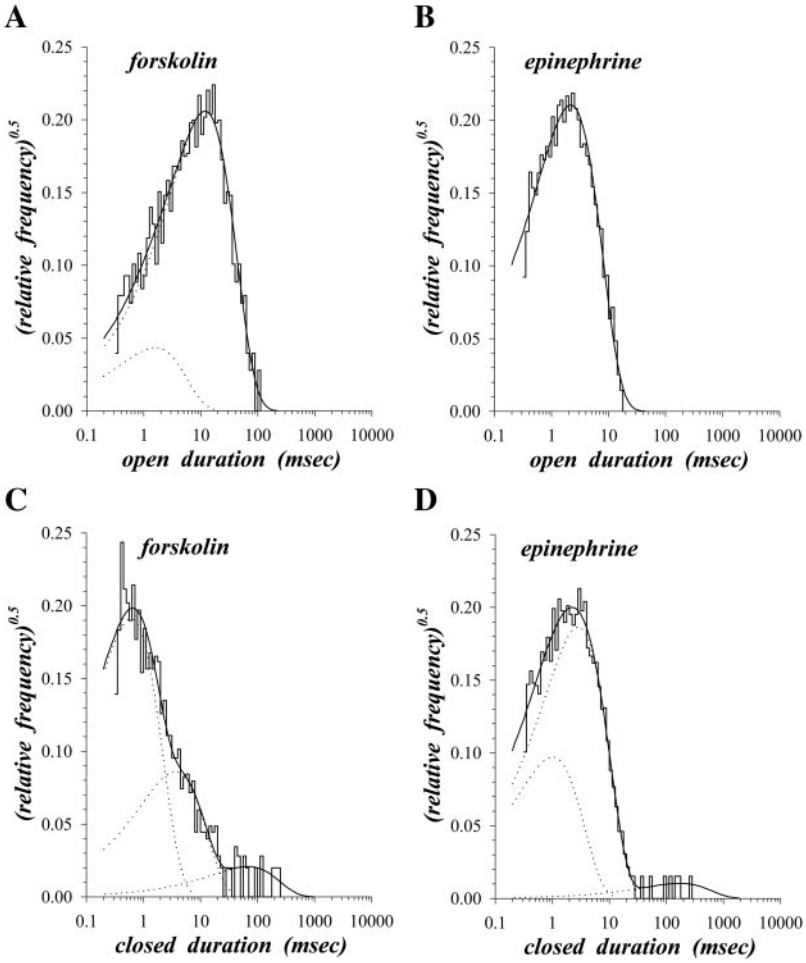

Fig. 12. Opening and closing kinetics for $^{gp}Cl_{or}$. Histograms are shown of open durations (*A* and *B*) and closed durations (*C* and *D*) with log binning (see METHODS) for single $^{gp}Cl_{or}$ during secretagogue stimulation while cell attached. V_{hold} was +60 mV. Each current record was ~20 s in length, with a large number of events in each condition: forskolin (1,512) and epinephrine (4,041). Open time histograms for forskolin condition had a peak fit well by a mixture of 2 exponentials; open time histograms for epinephrine condition had a peak fit best by a single exponential. Relative frequency was obtained by normalizing to the number of open events, estimated from the fitted exponentials. Individual fit components are shown as dotted lines. Fitted open time constants and proportions of events (in parentheses) were forskolin, 1.6 ms (0.04) and 11.9 ms (0.96); epinephrine, 2.2 ms. Closed time histograms exhibited multiple peaks requiring a mixture of exponentials for an adequate fit; relative frequency was obtained by normalizing to the number of open events for that condition. Fitted closed time constants and proportions of events (in parentheses) were forskolin, 0.6 ms (0.82), 3.6 ms (0.17), 67.9 ms (0.01); epinephrine, 1.0 ms (0.21), 2.8 ms (0.785), 171.6 ms (0.005).

Table 2. *Time constants for $^{gp}Cl_{or}$*

	O_S	O_L	C_1	C_2	C_3
Excised (n = 5)					
τ, ms	0.4 ± 0.03	22.5 ± 3.6	0.4 ± 0.05	2.3 ± 0.2	86.2 ± 31.1
Proportion	0.04 ± 0.06	0.96 ± 0.06	0.81 ± 0.02	0.16 ± 0.02	0.02 ± 0.01
Basal/forsk (n = 4)					
τ, ms	1.2 ± 0.1	10.2 ± 2.7*	0.4 ± 0.04	2.3 ± 0.4	100.8 ± 32.0
Proportion	0.09 ± 0.08	0.91 ± 0.08	0.75 ± 0.05	0.22 ± 0.05	0.02 ± 0.01
Epinephrine (n = 3)					
τ, ms		2.0 ± 0.2*	0.7 ± 0.2	2.0 ± 0.1*	76.4 ± 39.4
Proportion		1.00	0.28 ± 0.05	0.67 ± 0.12	0.04 ± 0.07

Shown are means ± SE of time constants (τ) and proportions of events for open (O_i) and closed (C_i) states of guinea pig outwardly rectifying Cl^- channels ($^{gp}Cl_{or}$). S, short duration; L, long duration. Voltage-dependent τ (*) are the values at +60 mV.

cates that the Cl^- channels observed in colonic crypts (Table 3) contributed to the exit pathway for Cl^-.

Conversion of transport function to active Cl^- secretion transforms cellular ion flow by redirecting Cl^- exit to apical membrane Cl^- channels. Colonic epithelia may contain separate cell types producing these two modes of ion secretion, but crypts respond to secretagogues with changes in cell composition, suggesting that both the electrogenic K^+ secretory mode and the electrogenic KCl secretory mode occur in columnar cells (24, 27). Cl^- permeability of colonic crypts is distinct between these modes, with a larger Cl^- efflux capacity in the K^+ secretory mode (24). For epithelial cells capable of producing both secretory modes, coordinated regulation of Cl^- channels in apical and basolateral membranes permits Cl^- exit to support either of these secretory modes. Although opening apical Cl^- channels is a key event for initiating Cl^- secretion, managing basolateral membrane Cl^- conductance (g_b^{Cl}) also would be necessary for the sustained ion secretion observed in colonic epithelia. Presumably, closing basolateral Cl^- channels would best serve promotion of Cl^- secretion, but cell volume control may necessitate specific amounts of g_b^{Cl}.

Basolateral membrane Cl^- channels. Two major Cl^- channel types were observed while cell attached on basolateral membrane of guinea pig distal colonic crypts (Figs. 1 and 2 and Table 3): outwardly rectified ($^{gp}Cl_{or}$) and linear ($^{gp}Cl_L$) *I-V* relations, with multiple conductance forms. Two conductance states likely exist within a single $^{gp}Cl_{or}$ type because patches with the larger-γ form of $^{gp}Cl_{or}$ had the smaller-γ form after excision (Fig. 4), even though outward currents were carried by 160 mM Cl^- from the pipette in both cases. Whether the three sizes of $^{gp}Cl_L$ (Fig. 2*B*) represent distinct channel types or simply were conductance states of a particular Cl^- channel cannot be resolved conclusively from the present data. However, voltage dependence of P_o also was different among the three $^{gp}Cl_L$ sizes (Fig. 9*B* and Table 3), supporting functionally distinct channel activities. Single-channel conductance (Fig. 2*B*) and voltage dependence of P_o (Fig. 9) can be used to compare these Cl^- channel activity patterns (Fig. 11*B*) with those of other Cl^- channel types.

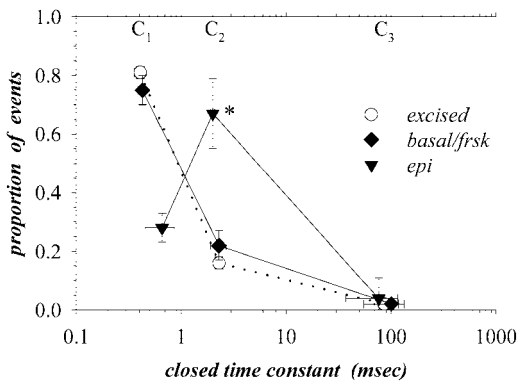

Fig. 13. Closed states for $^{gp}Cl_{or}$. Time constants and proportions of events for kinetic states obtained from fits of duration histograms to mixtures of exponentials were averaged from patches containing single $^{gp}Cl_{or}$ (Table 2). Basal and forskolin-stimulated cell-attached activity were similar and combined for averaging (◆; n = 4). Activity during epinephrine (▼; n = 3) and after excision (○; n = 5) also are shown. Asterisk indicates voltage-dependent time constant; value at +60 mV is shown.

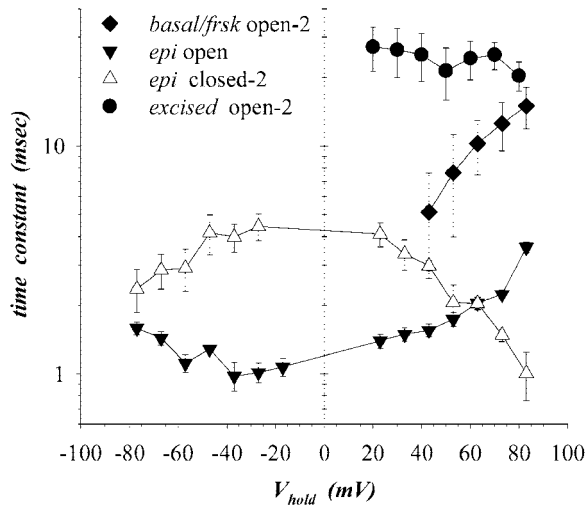

Fig. 14. Voltage dependence of time constants for $^{gp}Cl_{or}$. Open and closed kinetics were examined for patches with single $^{gp}Cl_{or}$ (as in Fig. 12). Dependence on V_{hold} of open time constants (τ_O) are shown for basal/forskolin (◆; n = 4), epinephrine (▼; n = 3), and excised (●; n = 4) conditions. Also shown is voltage dependence of τ_{C2} during epinephrine stimulation (△; n = 3).

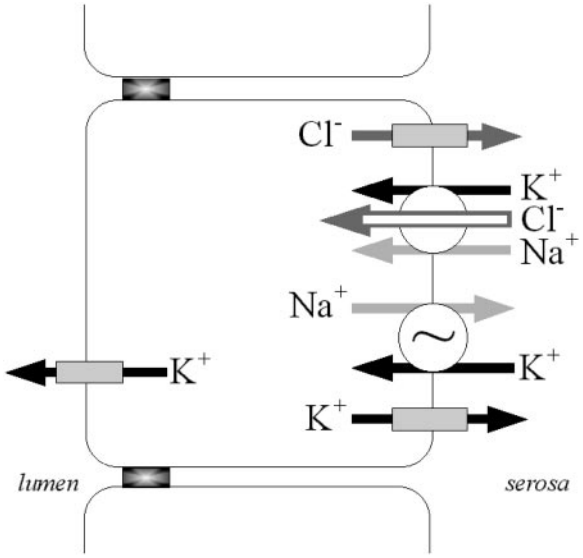

Fig. 15. Cellular transport model for electrogenic K^+ secretion. The proposed mechanism for electrogenic K^+ secretion across distal colonic epithelium includes 4 types of transport proteins (17, 50). Prevailing electrochemical gradients and phosphorylation potential determine the directions of net flow (arrows). The model schematic shows apical membrane K^+ channels acting in concert with a combination of basolateral membrane transporters (Na^+/K^+-ATPases, Na^+-K^+-$2Cl^-$ cotransporters, Cl^- channels, K^+ channels) that permit net K^+ uptake from the serosal interstitium into the cell and K^+ exit from the cell into the lumen. Positive charge flows across these epithelial cells from serosa to lumen carried by K^+ through apical membrane channels and by Cl^- through basolateral membrane channels. [The standard Cl^- secretory model (15, 18, 19) is similar, except that Cl^- channels dominate the apical membrane conductance and basolateral membrane Cl^- conductance would be assumed minimal.]

Cl_{or} has been observed in basolateral membranes of rat and mouse colonic crypts (3, 43) as well as mouse jejunal crypts (5). Those studies focused primarily on the cells at the base of the crypt near the stem cell, whereas the results reported here were from cells making up the cylindrical portion of the crypt where rapid cell division and secretion occur. The γ of $^{m}Cl_{or}$ in basolateral membranes of mouse colonic crypts (43) is similar to $^{gp}Cl_{or}$ at negative V_{hold} and at positive V_{hold} is intermediate to the two forms of $^{gp}Cl_{or}$ (Fig. 2*B*). Excision permits comparison of Cl_{or} under well-defined conditions of Cl^- concentration and V_m; at V_m = 0 mV and 160 mM Cl^-, γ is similar for $^{gp}Cl_{or}$, $^{m}Cl_{or}$, and $^{T84}Cl_{or}$: 47 (Fig. 3*B*), 36 (5, 43), and 41 (20, 26) pS, respectively. On the basis of outward rectification and ion selectivity, CLC-3 appears at present the most likely candidate for producing Cl_{or} (30, 46, 69) and therefore also $^{gp}Cl_{or}$.

P_o for Cl_{or} generally is larger at more positive V_{hold} in cell-attached recording (26, 37, 43), similar to $^{gp}Cl_{or}$ (Fig. 9*A*). Consequently, the time-averaged *I-V* relations for $^{gp}Cl_{or}$ were steeply rectified (Fig. 11). After excision this voltage dependence of P_o often is retained (26, 37, 43) but sometimes is lost (5, 48), as with $^{gp}Cl_{or}$ (Fig. 10*B*). Clearly, time-averaged currents would be less rectified with voltage-independent P_o. P_o for CLC-1 is largest at more positive V_m, with an equivalent gating charge of ~1 (33) similar to $^{gp}Cl_{or}$ (Fig. 9*A*); however, γ for CLC-1 is only ~2 pS (33). P_o for CLC-2 is largest at more negative V_m and for CLC-3 is relatively voltage independent (9, 33). This range of voltage sensitivities for CLC members suggests that this general channel structure could produce the characteristics of $^{gp}Cl_{or}$, but the exact features of $^{gp}Cl_{or}$ cannot be assigned conclusively to any of the CLC members.

Both $^{gp}Cl_{L21}$ and $^{gp}Cl_{L13}$ had voltage-independent γ with P_o that was larger at more positive V_{hold} (Figs. 2*C* and 9*B*). These conduction characteristics produce outwardly rectified time-averaged currents (Fig. 11*B*) that are similar to many Cl^- currents recorded in whole cell mode (16, 33, 47, 57, 62). The ~15-pS γ of CLCA is comparable to that of $^{gp}Cl_{L13}$ (16). A basolateral membrane Cl^- channel, with linear γ of 28 pS, activated by cell swelling in rat colonic crypts (12, 13), may correspond to $^{gp}Cl_{L21}$. Basolateral membrane Cl^- channels in kidney tubular cells have linear γ of 20–28 pS, and those from the thick ascending limb of Henle's loop have P_o that is larger at more positive V_m (53, 56). Although expression of CLC-K has only been demonstrated in the kidney and inner ear (33, 52, 55, 66), modest outward rectification of CLC-Kb/barttin whole cell current (66) is consistent with the behavior of $^{gp}Cl_{L21}$ (Fig. 11*B*).

The Cl^- channel formed by CFTR has voltage-independent γ of 6–10 pS (33, 60) as well as voltage-independent P_o (59). Both of these characteristics are consistent with $^{gp}Cl_{L8}$ behavior (Fig. 2*C*). However, CFTR has modestly outwardly rectified currents when recorded while cell attached compared with the linear *I-V* relation for $^{gp}Cl_{L8}$. As with the other $^{gp}Cl_L$, γ was voltage independent either because the low intracellular Cl^- concentration was saturating for conduction (consistent with relatively high-affinity Cl^- interaction in the pore) or currents would be modestly inwardly

Table 3. *Properties of $^{gp}Cl_{or}$ and $^{gp}Cl_L$*

	γ, pS	Voltage Dependence of γ	P_o	Voltage Dependence of P_o	K Secretagogue Action on *N*
$^{gp}Cl_{or}$	29.0	Rectified	0.20–0.40	Positive open	Increase
$^{gp}Cl_{L21}$	21.4	None	0.55	Positive open	Increase
$^{gp}Cl_{L13}$	13.2	None	0.35	Positive open	Increase
$^{gp}Cl_{L8}$	8.3	None	0.19 or 0.54	None	Increase

Shown are the means of single-channel conductance (γ) from Fig. 2 and open probability (P_o) from Fig. 9 for $^{gp}Cl_{or}$ and guinea pig Cl^- channel with linear current-voltage relation ($^{gp}Cl_L$) when cell attached at spontaneous cell membrane electrical potential difference (V_{cell}) [holding potential (V_{hold}) = O mV]. *N,* no. of channels.

rectified with equal Cl^- concentrations on both sides. For CFTR the outward rectification appears to include influences from phosphorylation and permeation by other intracellular anions (60). If $^{gp}Cl_{L8}$ were produced by CFTR, then other regulatory influences would be necessary to account for these differences in ion conduction. The voltage-independent steady-state conductance of CLC-Ka/barttin (66) also is consistent with the behavior of $^{gp}Cl_{L8}$.

Uncertainty concerning the molecular identity of $^{gp}Cl_{or}$ and $^{gp}Cl_L$ exists, in part, because the functional properties differ somewhat from those of presently defined Cl^- channel families. Channels observed in native tissue may occur as heteromultimeric assemblies of channel subunits together with regulatory components that produce distinct behavior. Combinations of CLC-1 and CLC-2 result in biophysical properties that are not a simple sum of the homomultimeric channels; in particular, voltage dependence is largely lost (41). The presence of the β-subunit barttin also alters the properties of CLC-K (66). Isolation of crypts may initiate a progressive alteration in channel subunits present such that biophysical and regulatory properties might change. However, colonic mucosa retains secretagogue sensitivity for K secretion for >8 h after isolation (51), and channel responses were similar over the ~36-h patch-clamp study period. Species-dependent differences in channel function also may contribute to difficulty in precisely identifying these guinea pig Cl^- channels. Although the identities of the Cl^- channels observed in this study remain undetermined, a basolateral location does allow contributions to cell functions ranging from cell volume control to transepithelial ion flow.

Regulation of K^+ secretion. Control of g_b^{Cl} contributes to determining the rate of electrogenic K^+ secretion by providing an exit path for Cl^- entering via Na^+-K^+-$2Cl^-$ cotransporters (Fig. 15) and by influencing the electrical driving force for apical K^+ exit. The Cl^- channels $^{gp}Cl_{or}$ and $^{gp}Cl_L$ (Table 3) are likely involved in augmenting this g_b^{Cl} needed for K^+ secretion. Stimulation of electrogenic K^+ secretion occurs through β-adrenergic receptors (17) and prostaglandin EP_2 receptors (23), both of which act through increasing intracellular cAMP. Activation of prostaglandin DP receptors, which also increase cAMP production, stimulates electrogenic KCl secretion (23), suggesting a functional compartmentalization of cAMP allowing selective induction of Cl^- secretion. The concentration dependence of the forskolin response supports the existence of two interactions with distinct affinity (Fig. 5*B*) similar to adenylyl cyclase activation in human colonic crypts (4). This divergence of sensitivities to forskolin may represent distinct forms of adenylyl cyclase, because activation with the G protein $G_S\alpha$ increases forskolin affinity of adenylyl cyclase from an EC_{50} of >10 μM to ~100 nM (64). Specific activation of Cl^- channels to support each ion secretory mode may occur via adenylyl cyclases that are functionally compartmentalized through the action of other intracellular signaling cascades.

Secretagogues for electrogenic K^+ secretion, epinephrine and either PGE_2 or forskolin at low concentration, increased the number of active $^{gp}Cl_{or}$ and $^{gp}Cl_L$ (Table 3), consistent with higher g_b^{Cl}. The epinephrine secretory state of $^{gp}Cl_{or}$ had lower P_o due to a shift in the P_o voltage dependence to more positive V_{hold} (Fig. 9*A*). $^{gp}Cl_{L13}$ also supported secretagogue activation of g_b^{Cl} with increased P_o at the spontaneous V_{cell} (Fig. 9*B*). In addition, high-concentration PGE_2 that stimulates Cl^- secretion (23, 50) appeared to decrease N for $^{gp}Cl_{or}$ (Fig. 7*B*) such that g_b^{Cl} would be reduced. Cholinergic stimulation of a Cl^- secretory state increased flickering of $^{gp}Cl_{or}$, consistent with reduced P_o (Fig. 7*B*). GTP induced a similar flickery state with reduced current amplitude in $^{m}Cl_{or}$ excised from colonic crypts (43). Overall, K^+ secretagogues increased N for $^{gp}Cl_{or}$ and $^{gp}Cl_L$, but epinephrine produced a distinct secretory mode for $^{gp}Cl_{or}$ with lower P_o than with forskolin (Fig. 9*A*). Therefore, other intracellular signals in addition to cAMP may be needed to regulate the basolateral membrane Cl^- channels involved in electrogenic K^+ secretion.

Kinetic analysis of $^{gp}Cl_{or}$ activity (Figs. 12, 13, and 14) provided further insight into regulation of K^+ secretion. Epinephrine activation of $^{gp}Cl_{or}$ occurred with flickery kinetics distinct from basally active or forskolin-activated channels (Figs. 6 and 7). Open durations were shorter (Fig. 12 and Table 2), and closed durations were dominated by events with a medium-length τ (Figs. 12 and 13 and Table 2), leading to a shift in the voltage dependence of P_o (Fig. 9*B*). Absence of the flickery epinephrine mode in the presence of forskolin (Fig. 7*B*) suggested that a basal/forskolin-induced factor can suppress entry into this flickery kinetic mode. Because excision of patches with $^{gp}Cl_{or}$ in the flickery mode led to slower kinetics similar to the basal/forskolin mode (Fig. 10 and Table 2), a component of this kinetic control factor apparently was readily exchangeable. Excision of patches also led to a loss of voltage dependence for P_o (Fig. 10) and reduction in γ at positive V_m (Fig. 4), consistent with readily exchangeable regulators.

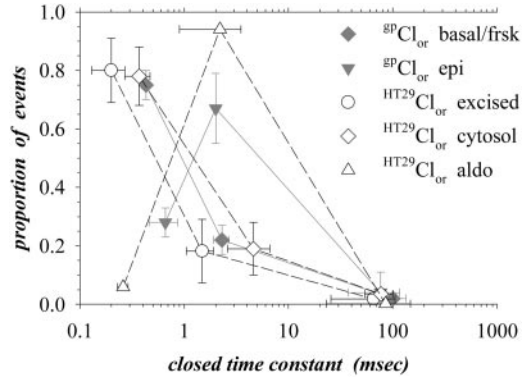

Fig. 16. Regulation of closed states for Cl_{or}. Time constants and proportions of events for kinetic states are shown for $^{gp}Cl_{or}$ (Fig. 13) and Cl_{or} recorded from the human colonic tumor cell line HT29 (49). All kinetic constants for $^{HT29}Cl_{or}$ are from excised I/O patches; aldosterone (100 μM) and cytosol were added to the bath solution.

Activation of Cl_{or} after excision is a general observation in many cell types (3, 5, 26, 30, 33, 43, 61), supporting the existence of cytosolic inhibitory regulators (35, 36, 38). The exact nature of these regulators is presently unknown, but several classes of compounds have been implicated. Extracts of cytosol appear to contain both a high-molecular-mass (10–300 kDa) substance, likely a protein, and a lower-molecular-mass (<1 kDa) substance similar to steroids (36). Addition of cytosol to excised $^{HT29}Cl_{or}$ reduces τ_O from 32 to 7 ms (49), similar to the difference between excised and basal/forskolin modes for $^{gp}Cl_{or}$ (Table 2). Closed τ for $^{HT29}Cl_{or}$ are essentially unchanged by cytosol (49) similar to excised and basal/forskolin modes for $^{gp}Cl_{or}$ (Figs. 13 and 16). Fatty acids such as arachidonic acid can reduce P_o of Cl_{or}, but the mode of action and molecular size suggest that the inhibitor present in cytosol is distinct (31, 36, 38).

The flickery nature of the epinephrine-induced mode for $^{gp}Cl_{or}$ can be mimicked in excised $^{HT29}Cl_{or}$ by aldosterone or glibenclamide (48, 49); τ_O is reduced to ~1 ms, and events with τ_C of ~2 ms dominate closures (Fig. 16). The high EC_{50} for aldosterone action (~20 μM) led Rabe and Frömter (49) to suggest that another lipid component may be the actual endogenous control component. Both aldosterone and glibenclamide are proposed to act by moving $^{HT29}Cl_{or}$ into a specific kinetic mode rather than by blocking (48, 49), which was supported by the action of the secretagogue epinephrine to induce a nearly identical kinetic mode in $^{gp}Cl_{or}$ (Fig. 16 and Table 2). Furthermore, such a steroidlike lipid may be the specific mediator of epinephrine activation.

Secretory control of $^{gp}Cl_{or}$ and $^{gp}Cl_L$ included increased N and P_o such that a range of g_b^{Cl} was possible. Each of these Cl^- channel activities may contribute a unique set of regulatory responses to adjust for demands on secretory rate and cell volume control. Regulatory subunits associating with the observed Cl^- channels may be necessary to produce the specific types of secretagogue sensitivities. The CLC-K β-subunit barttin promotes channel activity (66), and subunits alter responsiveness of K^+ channels to cytoplasmic signals. In particular, CFTR belongs to a protein family that includes the sulfonylurea receptor that confers ATP sensitivity to K^+ channels, and CFTR has been shown to associate with K^+ channels (54). The coincident presence of $^{gp}K_{ir}$ with $^{gp}Cl_{or}$ (Fig. 1*A*) and $^{gp}Cl_L$ suggests that a tight regulatory connection potentially could exist between g_b^K and g_b^{Cl} in colonic crypts. Similarly, association of $^{gp}Cl_L$ with $^{gp}Cl_{or}$ might confer control like that between CFTR and Cl_{or} (30).

A basolateral membrane location of Cl^- channels in epithelia presumably serves both volume-regulatory needs and transepithelial flow requirements. Whether volume-activated channels open during K^+ secretion was not determined in the present study, but conductive Cl^- exit would aid maintenance of cell volume during secretory stimulation of Cl^- influx through Na^+-K^+-$2Cl^-$ cotransporters. As noted numerous times, transepithelial solute flow combines aspects of regulatory volume increase (RVI) and regulatory volume decrease (RVD). The distinct situation in epithelia, as during electrogenic K^+ secretion (Fig. 15), is that cell volume is maintained near control values while transport processes resembling RVI and RVD remain active. Simultaneous and continual operation of influx and efflux pathways is what produces sustained transepithelial flow. Thus a complete control scheme for basolateral Cl^- channels will include not only the initiating events but also the modulating signals that ensure stable cellular conditions during ongoing secretion.

This study was supported by grants from the National Institute of Diabetes and Digestive and Kidney Diseases (DK-39007) and the Wright State University Research Challenge Program.

REFERENCES

1. **Barry PH and Lynch JW.** Liquid junction potentials and small cell effects in patch-clamp analysis. *J Membr Biol* 121: 101–117, 1991.
2. **Bjerknes M and Cheng H.** Methods for the isolation of intact epithelium from the mouse intestine. *Anat Rec* 199: 565–574, 1981.
3. **Bleich M, Riedemann N, Warth R, Kerstan D, Leipziger J, Hör M, Van Driessche W, and Greger R.** Calcium regulated potassium and non-selective cation channels in the basolateral membrane of rat colonic crypt base cells. *Pflügers Arch* 432: 1011–1022, 1996.
4. **Boige N, Amiranoff B, Munck A, and Laburthe M.** Forskolin stimulates adenylate cyclase in human colonic crypts: interaction with VIP. *Eur J Pharmacol* 101: 111–117, 1984.
5. **Butt AG and Hamilton KL.** Ion channels in isolated mouse jejunal crypts. *Pflügers Arch* 435: 528–538, 1998.
6. **Carew MA and Thorn P.** Carbachol-stimulated chloride secretion in mouse colon: evidence of a role for autocrine prostaglandin-E_2 release. *Exp Physiol* 85: 67–72, 2000.
7. **Catalán M, Cornejo I, Figueroa CD, Niemeyer MI, Sepúlveda FV, and Cid LP** CLC-2 in guinea pig colon: mRNA, immunolabeling, and functional evidence for surface epithelium localization. *Am J Physiol Gastrointest Liver Physiol* 283: G1004–G1013, 2002.
8. **Chang EB and Rao MC.** Intestinal water and electrolyte transport: mechanisms of physiological and adaptive responses. *Physiology of the Gastrointestinal Tract*, edited by Johnson LR. New York: Raven, 1994, p.2027–2081.
9. **Cid LP, Niemeyer MI, Ramirez A, and Sepúlveda FV.** Splice variants of a CLC-2 chloride channel with differing functional characteristics. *Am J Physiol Cell Physiol* 279: C1198–C1210, 2000.
10. **Cohn JA, Melhus O, Page LJ, Dittrich KL, and Vigna SR.** CFTR: development of high-affinity antibodies and localization in sweat gland. *Biochem Biophys Res Commun* 181: 36–43, 1991.
11. **Cuthbert AW, MacVinish LJ, Hickman ME, Ratcliff R, Colledge WH, and Evans MJ.** Ion-transporting activity in the murine colonic epithelium of normal animals and animals with cystic fibrosis. *Pflügers Arch* 428: 508–515, 1994.
12. **Diener M, Nobles M, and Rummel W.** Activation of basolateral Cl channels in the rat colonic epithelium during regulatory volume decrease. *Pflügers Arch* 421: 530–538, 1992.
13. **Diener M, Rummel W, Mestres P, and Lindemann B.** Single chloride channels in colon mucosa and isolated colonic enterocytes of the rat. *J Membr Biol* 108: 21–30, 1989.
14. **Dwyer TM.** A patch clamp primer. *J Electrophysiol Techniques* 12: 15–29, 1985.
15. **Frizzell RA and Halm DR.** Chloride channels in epithelial cells. In: *Current Topics in Membranes and Transport: Channels and Noise in Epithelial Tissues*, edited by Bronner F, Helman SI, and Van Driessche W. San Diego: Academic, 1990, vol. 37, p. 247–282.

16. **Gruber AD, Fuller CM, Elble RC, Benos DJ, and Pauli BU.** The CLCA gene family: a novel family of putative chloride channels. *Curr Genomics* 1: 201–222, 2000.
17. **Halm DR and Frizzell RA.** Active potassium transport across rabbit distal colon: relation to sodium absorption and chloride secretion. *Am J Physiol Cell Physiol* 251: C252–C267, 1986.
18. **Halm DR and Frizzell RA.** Intestinal chloride secretion. In: *Textbook of Secretory Diarrhea*, edited by Lebenthal E and Duffey M. New York: Raven, 1990, p. 47–58.
19. **Halm DR and Frizzell RA.** Ion transport across the large intestine. *Handbook of Physiology. The Gastrointestinal System. Intestinal Absorption and Secretion*. Bethesda, MD: Am. Physiol. Soc., 1991, sect. 6, vol. IV, chapt. 8, p. 257–274.
20. **Halm DR and Frizzell RA.** Anion permeation in an apical membrane chloride channel of a secretory epithelial cell. *J Gen Physiol* 99: 333–362, 1992.
21. **Halm DR and Halm ST.** Aldosterone stimulates potassium secretion prior to onset of sodium absorption in guinea pig distal colon. *Am J Physiol Cell Physiol* 266: C552–C558, 1994.
22. **Halm DR and Halm ST.** Secretagogue response of goblet cells and columnar cells in human colonic crypts. *Am J Physiol Cell Physiol* 277: C501–C522, 1999. [Corrigenda. *Am J Physiol Cell Physiol* 278: C212–C233, 2000].
23. **Halm DR and Halm ST.** Prostanoids stimulate K secretion and Cl secretion in guinea pig distal colon via distinct pathways. *Am J Physiol Gastrointest Liver Physiol* 281: G984–G996, 2001.
24. **Halm DR, Kirk KL, and Sathiakumar KC.** Stimulation of chloride permeability in colonic crypts of Lieberkühn measured with a fluorescent indicator. *Am J Physiol Gastrointest Liver Physiol* 265: G423–G431, 1993.
25. **Halm DR, Krasny EJ Jr, and Frizzell RA.** Electrophysiology of flounder intestinal mucosa: I. Conductance properties of the cellular and paracellular pathways. *J Gen Physiol* 85: 843–864, 1985.
26. **Halm DR, Rechkemmer G, Schoumacher RA, and Frizzell RA.** Apical membrane chloride channels in a colonic cell line activated by secretory agonists. *Am J Physiol Cell Physiol* 254: C505–C511, 1988.
27. **Halm DR and Rick R.** Secretion of potassium and chloride across colonic epithelium: cellular localization using electron microprobe analysis. *Am J Physiol Cell Physiol* 262: C1001–C1011, 1992.
28. **Hille B.** *Ion Channels of Excitable Membranes* (3rd ed). Sunderland, MA: Sinauer Associates, 2001, p. 814.
29. **Horn R.** Estimating the number of channels in patch recordings. *Biophys J* 60: 433–439, 1991.
30. **Hryciw DH and Guggino WB.** Cystic fibrosis transmembrane conductance regulator and the outwardly rectifying chloride channel: a relationship between two chloride channels expressed in epithelial cells. *Clin Exp Pharmacol Physiol* 27: 892–895, 2000.
31. **Hwang T, Guggino SE, and Guggino WB.** Direct modulation of secretory chloride channels by arachidonic and other *cis* unsaturated fatty acids. *Proc Natl Acad Sci USA* 87: 5706–5709, 1990.
32. **Jackson MB.** Stationary single-channel analysis. *Methods Enzymol* 207: 729–746, 1992.
33. **Jentsch TJ, Stein V, Weinreich F, and Zdebik AA.** Molecular structure and physiological function of chloride channels. *Physiol Rev* 82: 503–568, 2002.
34. **Kartner N, Augustinas O, Jensen TJ, Naismith AL, and Riordan JR.** Mislocalization of ΔF508 CFTR in cystic fibrosis sweat gland. *Nat Genet* 1: 321–327, 1992.
35. **Krick W, Disser J, Hazama A, Burckhardt G, and Greger R.** Evidence for a cytosolic inhibitor of epithelial chloride channels. *Pflügers Arch* 418: 491–499, 1991.
36. **Krick W, Disser J, Rabe A, Frömter E, Hansen CP, Roch B, Kunzelmann K, Greger R, Fehlhaber H, and Burckhardt G.** Characterization of cytosolic Cl channel inhibitors by size exclusion chromatography. *Cell Physiol Biochem* 5: 259–268, 1995.
37. **Krouse ME, Hagiwara G, Chen J, Lewiston NJ, and Wine JJ.** Ion channels in normal human and cystic fibrosis sweat gland cells. *Am J Physiol Cell Physiol* 257: C129–C140, 1989.
38. **Kunzelmann K, Tilmann M, Hansen CP, and Greger R.** Inhibition of epithelial chloride channels by cytosol. *Pflügers Arch* 418: 479–490, 1991.
39. **Li Y and Halm DR.** Secretory modulation of basolateral membrane inwardly rectified K channel in guinea pig distal colonic crypts. *Am J Physiol Cell Physiol* 282: C719–C735, 2002.
40. **Lipecka J, Bali M, Thomas A, Fanen P, Edelman A, and Fritsch J.** Distribution of CLC-2 chloride channel in rat and human epithelial tissues. *Am J Physiol Cell Physiol* 282: C805–C816, 2002.
41. **Lorenz C, Pusch M, and Jentsch TJ.** Heteromultimeric CLC chloride channels with novel properties. *Proc Natl Acad Sci USA* 93: 13362–13366, 1996.
42. **Lohrmann E and Greger R.** Isolated perfused rabbit colon crypts: stimulation of Cl secretion by forskolin. *Pflügers Arch* 425: 373–380, 1993.
43. **Mignen O, Egee S, Liberge M, and Harvey BJ.** Basolateral outward rectifier chloride channel in isolated crypts of mouse colon. *Am J Physiol Gastrointest Liver Physiol* 279: G277–G287, 2000.
44. **Mohammad-Panah R, Ackerley C, Rommens J, Choudhury M, Wang Y, and Bear CE.** The chloride channel CLC-4 colocalizes with cystic fibrosis transmembrane conductance regulator and may mediate chloride flux across the apical membrane of intestinal epithelia. *J Biol Chem* 277: 566–574, 2002.
45. **Neher E.** Correction for liquid junction potential in patch clamp experiments. *Methods Enzymol* 207: 123–131, 1992.
46. **Ogura T, Furukawa T, Toyozaki T, Yamada K, Zheng YJ, Katayama Y, Nakaya H, and Inagaki N.** ClC-3B, a novel ClC-3 splicing variant that interacts with EBP50 and facilitates expression of CFTR-regulated ORCC. *FASEB J* 16: 863–865, 2002.
47. **Okada Y.** Volume expansion-sensing outward-rectifier Cl channel: fresh start to the molecular identity and volume sensor. *Am J Physiol Cell Physiol* 273: C755–C789, 1997.
48. **Rabe A, Disser J, and Frömter E.** Cl channel inhibition by glibenclamide is not specific for the CFTR-type Cl channel. *Pflügers Arch* 429: 659–662, 1995.
49. **Rabe A and Frömter E.** Micromolar concentrations of steroids and of aldosterone antagonists inhibit the outwardly rectifying chloride channels with different kinetics. *Pflügers Arch* 439: 559–566, 2000.
50. **Rechkemmer G, Frizzell RA, and Halm DR.** Active potassium transport across guinea pig distal colon: action of secretagogues. *J Physiol* 493: 485–502, 1996.
51. **Rechkemmer G and Halm DR.** Aldosterone stimulates potassium secretion across mammalian colon independent of sodium absorption. *Proc Natl Acad Sci USA* 86: 397–401, 1989.
52. **Reeves WB, Winters CJ, and Andreoli TE.** Chloride channels in the loop of Henle. *Annu Rev Physiol* 63: 631–645, 2001.
53. **Reeves WB, Winters CJ, Filipovic DM, and Andreoli TE.** Cl channels in basolateral renal medullary vesicles. IX. Channels from mouse MTAL cell patches and medullary vesicles. *Am J Physiol Renal Fluid Electrolyte Physiol* 269: F621–F627, 1995.
54. **Ruknudin A, Schulze DH, Sullivan SK, and Welling PA.** Novel subunit composition of a renal epithelial K_{ATP} channel. *J Biol Chem* 273: 14165–14171, 1998.
55. **Sage CL and Marcus DC.** Immunolocalization of CLC-K chloride channel in stria marginal cells and vestibular dark cells. *Hear Res* 160: 1–9, 2001.
56. **Sansom SC, La B, and Carosi SL.** Double-barreled chloride channels of collecting duct basolateral membrane. *Am J Physiol Renal Fluid Electrolyte Physiol* 259: F46–F52, 1990.
57. **Schultheiss G and Diener M.** Potassium and chloride conductances in the distal colon of the rat. *Gen Pharmacol* 31: 337–342, 1998.
58. **Schultz BD, Singh AK, Devor DC, and Bridges RJ.** Pharmacology of CFTR chloride channel activity. *Physiol Rev* 79: S109–S144, 1999.
59. **Shepard DN and Robinson KA.** Mechanism of glibenclamide inhibition of cystic fibrosis transmembrane regulator Cl channel expressed in a murine cell line. *J Physiol* 503: 333–346, 1997.
60. **Shepard DN and Welsh MJ.** Structure and function of the CFTR chloride channel. *Physiol Rev* 79: S23–S45, 1999.

61. **Solc CK and Wine JJ.** Swelling-induced and depolarization-induced Cl channels in normal and cystic fibrosis epithelial cells. *Am J Physiol Cell Physiol* 261: C658–C674, 1991.
62. **Strange K, Emma F, and Jackson PS.** Cellular and molecular physiology of volume-sensitive anion channels. *Am J Physiol Cell Physiol* 270: C711–C730, 1996.
63. **Strong TV, Boehm K, and Collins FS.** Localization of cystic fibrosis transmembrane conductance regulator mRNA in the human gastrointestinal tract by in situ hybridization. *J Clin Invest* 93: 347–354, 1994.
64. **Sunahara RK, Dessauer CW, Whisnant RE, Kleuss C, and Gilman AG.** Interaction of $G_{s\alpha}$ with the cytosolic domains of mammalian adenylyl cyclase. *J Biol Chem* 272: 22265–22271, 1997.
65. **Vandewalle A, Cluzeaud F, Peng K, Bens M, Lüchow A, Günther W, and Jentsch TJ.** Tissue distribution and subcellular localization of the CLC-5 chloride channel in rat intestinal cells. *Am J Physiol Cell Physiol* 280: C373–C381, 2001.
66. **Waldegger S, Jeck N, Barth P, Peters M, Vitzthum H, Wolf K, Kurtz A, Konrad M, and Seyberth HW.** Barttin increases surface expression and changes current properties of CLC-K channels. *Pflügers Arch* 444: 411–418, 2002.
67. **Wangemann P.** Comparison of ion transport mechanisms between vestibular dark cells and strial marginal cells. *Hear Res* 90: 149–157, 1995.
68. **Wegmann M, Kämpen A, Weber S, Seyberth HW, and Köckerling A.** Effect of hydroxyeicosatetraenoic acids on furosemide-sensitive chloride secretion in rat distal colon. *J Pharmacol Exp Ther* 295: 133–138, 2000.
69. **Wills NK and Fong P.** CLC chloride channels in epithelia: recent progress and remaining puzzles. *News Physiol Sci* 16: 161–166, 2001.